observed in the present study were M2c microglia. However, the subtypes of M2 cells have not been referred to in studies on SCI. The present study also did not investigate the properties of the M2 cells; further studies will be required to clarify the properties of the M2 subtypes that are activated following SCI. In addition, it should be mentioned that we cannot conclude that IL-10 is the primary M2-polarizing signal induced following LPS preconditioning. A more extensive array analysis would be required to determine the hierarchy of M2 regulation.

TLR4, a receptor of LPS, binds to two main adapter proteins, MyD88 and TRIF, which independently activate the MyD88–NFκB pathway and TRIF–IRF pathway, respectively (Yamamoto et al., 2003). IRF-3 is activated via LPS–TLR4 signals through the TRIF–IRF pathway (Honda and Taniguchi, 2006). In vitro studies have shown that IRF-3-deficient macrophages fail to induce ET (Biswas et al., 2007). In stroke models, LPS preconditioning induces IRF-3 activation via the redirection of TLR4 signaling (Stevens et al., 2011; Vartanian et al., 2011). The present study confirmed that IRF-3 activation was induced within 12 hr of SCI as a result of LPS preconditioning, which is in line with the results from the stroke model. Additionally, we found that increased IRF-3 activity as a result of the LPS preconditioning was concurrent with increased IL-10 gene expression. These results are in line with findings reported by Samanta et al. (2008) and Biswas and Lopez-Collazo (2009) that IL-10 expression is directly and indirectly regulated by IRF-3. Overall, given these results, we speculate that the M2 redirection that occurred as a result of the LPS preconditioning was induced via LPS–TLR4 signals through the TRIF–IRF pathway and led to increased IL-10 expression.

Treatment with IL-10 has been widely studied in SCI models and shown to exert a therapeutic effect through systemic administration of the protein, in combination with cell grafts, or through local gene delivery (Brewer et al., 1999; Thompson et al., 2013). However, complications with IL-10 therapy, such as infection at the surgical site resulting from continuous administration of IL-10 or polyneuropathy, are unavoidable (van der Poll et al., 1996; Dace et al., 2009). LPS preconditioning would be a convenient method for inducing M2 activation through enhanced IL-10 expression with a single LPS injection. However, it is not accurate to compare IL-10 therapy and LPS preconditioning because molecules other than IL-10 might additionally contribute to the effect of LPS preconditioning.

In clinical situations, it might be difficult to apply LPS preconditioning directly to SCI because injuries occur before patients arrive at the hospital. However, it is feasible to apply LPS preconditioning prophylactically before events such as delicate spine surgery that pose a high risk with respect to SCI. Postconditioning is a promising approach that could be applied to clinical SCI, although few studies in ischemic models have been reported (Mockford et al., 2009). Further studies are required before LPS preconditioning can be applied in clinical settings.

In conclusion, we found that LPS preconditioning has a therapeutic effect on CNS microglia following SCI through the modulation of M1/M2 polarization. The present study provides new insights into the effects of endotoxin preconditioning on the CNS immune system. Further studies are required before practical application of LPS treatment in clinical settings; however, this study suggests that modulation of the CNS immune system through endotoxin preconditioning could be widely applicable for many CNS diseases in which inflammation occurs.

ACKNOWLEDGMENTS

We thank M. Nagao, Y. Ichihara, S. Iwama, and N. Kume for technical assistance and K. Nakanishi for secretarial assistance. The authors have no competing financial interests.

REFERENCES

Basso DM, Fisher LC, Anderson AJ, Jakeman LB, McTigue DM, Popovich PG. 2006. Basso Mouse Scale for locomotion detects differences in recovery after spinal cord injury in five common mouse strains. J Neurotrauma 23:635–659.

Bell MT, Puskas F, Agoston VA, Cleveland JC Jr, Freeman KA, Gamboni F, Herson PS, Meng X, Smith PD, Weyant MJ, Fullerton DA, Reece TB. 2013. Toll-like receptor 4-dependent microglial activation mediates spinal cord ischemia–reperfusion injury. Circulation 128: S152–S156.

Bethea JR, Dietrich WD. 2002. Targeting the host inflammatory response in traumatic spinal cord injury. Curr Opin Neurol 15:355–360.

Biswas SK, Lopez-Collazo E. 2009. Endotoxin tolerance: new mechanisms, molecules and clinical significance. Trends Immunol 30:475–487.

Biswas SK, Bist P, Dhillon MK, Kajiji T, Del Fresno C, Yamamoto M, Lopez-Collazo E, Akira S, Tergaonkar V. 2007. Role for MyD88-independent, TRIF pathway in lipid A/TLR4-induced endotoxin tolerance. J Immunol 179:4083–4092.

Brewer KL, Bethea JR, Yezierski RP. 1999. Neuroprotective effects of interleukin-10 following excitotoxic spinal cord injury. Exp Neurol 159:484–493.

Chen KB, Uchida K, Nakajima H, Yayama T, Hirai T, Rodriguez Guerrero A, Kobayashi S, Ma WY, Liu SY, Zhu P, Baba H. 2011. High-mobility group box-1 and its receptors contribute to proinflammatory response in the acute phase of spinal cord injury in rats. Spine 36:2122–2129.

Chen Z, Jalabi W, Shpargel KB, Farabaugh KT, Dutta R, Yin X, Kidd GJ, Bergmann CC, Stohlman SA, Trapp BD. 2012. Lipopolysaccharide-induced microglial activation and neuroprotection against experimental brain injury is independent of hematogenous TLR4. J Neurosci 32:11706–11715.

Dace DS, Khan AA, Stark JL, Kelly J, Cross AH, Apte RS. 2009. Interleukin-10 overexpression promotes Fas-ligand-dependent chronic macrophage-mediated demyelinating polyneuropathy. PloS One 4: e7121.

David S, Kroner A. 2011. Repertoire of microglial and macrophage responses after spinal cord injury. Nat Rev Neurosci 12:388–399.

Dirnagl U, Becker K, Meisel A. 2009. Preconditioning and tolerance against cerebral ischaemia: from experimental strategies to clinical use. Lancet Neurol 8:398–412.

Fan H, Cook JA. 2004. Molecular mechanisms of endotoxin tolerance. J Endotoxin Res 10:71–84.

Fleming JC, Norenberg MD, Ramsay DA, Dekaban GA, Marcillo AE, Saenz AD, Pasquale-Styles M, Dietrich WD, Weaver LC. 2006. The cellular inflammatory response in human spinal cords after injury. Brain 129:3249–3269.

Honda K, Taniguchi T. 2006. IRFs: master regulators of signaling by toll-like receptors and cytosolic pattern-recognition receptors. Nat Rev Immunol 6:644–658.

Jetten N, Verbruggen S, Gijbels MJ, Post MJ, De Winther MP, Donners MM. 2014. Anti-inflammatory M2, but not proinflammatory M1, macrophages promote angiogenesis in vivo. Angiogenesis 17:109–118.

Kamei N, Kwon SM, Kawamoto A, Ii M, Ishikawa M, Ochi M, Asahara T. 2012. Contribution of bone marrow-derived endothelial progenitor cells to neovascularization and astrogliosis following spinal cord injury. J Neurosci Res 90:2281–2292.

Kigerl KA, Lai W, Rivest S, Hart RP, Satoskar AR, Popovich PG. 2007. Toll-like receptor (TLR)-2 and TLR-4 regulate inflammation, gliosis, and myelin sparing after spinal cord injury. J Neurochem 102: 37–50.

Kigerl KA, Gensel JC, Ankeny DP, Alexander JK, Donnelly DJ, Popovich PG. 2009. Identification of two distinct macrophage subsets with divergent effects causing either neurotoxicity or regeneration in the injured mouse spinal cord. J Neurosci 29:13435–13444.

Kim HM, Hwang DH, Lee JE, Kim SU, Kim BG. 2009. Ex vivo VEGF delivery by neural stem cells enhances proliferation of glial progenitors, angiogenesis, and tissue sparing after spinal cord injury. PloS One 4: e4987.

Kodelja V, Muller C, Tenorio S, Schebesch C, Orfanos CE, Goerdt S. 1997. Differences in angiogenic potential of classically vs alternatively activated macrophages. Immunobiology 197:478–493.

Lastres-Becker I, Cartmell T, Molina-Holgado F. 2006. Endotoxin preconditioning protects neurones from in vitro ischemia: role of endogenous IL-1beta and TNF-alpha. J Neuroimmunol 173:108–116.

Leow-Dyke S, Allen C, Denes A, Nilsson O, Maysami S, Bowie AG, Rothwell NJ, Pinteaux E. 2012. Neuronal Toll-like receptor 4 signaling induces brain endothelial activation and neutrophil transmigration in vitro. J Neuroinflamm 9:230.

Li WC, Jiang DM, Hu N, Qi XT, Qiao B, Luo XJ. 2013. Lipopolysaccharide preconditioning attenuates neuroapoptosis and improves functional recovery through activation of Nrf2 in traumatic spinal cord injury rats. Int J Neurosci 123:240–247.

Lin HY, Huang CC, Chang KF. 2009. Lipopolysaccharide preconditioning reduces neuroinflammation against hypoxic ischemia and provides long-term outcome of neuroprotection in neonatal rat. Pediatr Res 66: 254–259.

Longhi L, Gesuete R, Perego C, Ortolano F, Sacchi N, Villa P, Stocchetti N, De Simoni MG. 2011. Long-lasting protection in brain trauma by endotoxin preconditioning. J Cereb Blood Flow Metab 31: 1919–1929.

Mantovani A, Sozzani S, Locati M, Allavena P, Sica A. 2002. Macrophage polarization: tumor-associated macrophages as a paradigm for polarized M2 mononuclear phagocytes. Trends Immunol 23:549–555.

Mockford KA, Girn HR, Homer-Vanniasinkam S. 2009. Postconditioning: current controversies and clinical implications. Eur J Vasc Endovasc Surg 37:437–442.

Mosser DM, Edwards JP. 2008. Exploring the full spectrum of macrophage activation. Nat Rev Immunol 8:958–969.

Nikodemova M, Small AL, Smith SM, Mitchell GS, Watters JJ. 2013. Spinal but not cortical microglia acquire an atypical phenotype with high VEGF, galectin-3 and osteopontin, and blunted inflammatory responses in ALS rats. Neurobiol Dis 69:43–53.

Nishimura S, Yasuda A, Iwai H, Takano M, Kobayashi Y, Nori S, Tsuji O, Fujiyoshi K, Ebise H, Toyama Y, Okano H, Nakamura M. 2013. Time-dependent changes in the microenvironment of injured spinal cord affects the therapeutic potential of neural stem cell transplantation for spinal cord injury. Mol Brain 6:3.

Okada S, Nakamura M, Katoh H, Miyao T, Shimazaki T, Ishii K, Yamane J, Yoshimura A, Iwamoto Y, Toyama Y, Okano H. 2006. Conditional ablation of Stat3 or Socs3 discloses a dual role for reactive astrocytes after spinal cord injury. Nat Med 12:829–834.

Popovich PG, Guan Z, McGaughy V, Fisher L, Hickey WF, Basso DM. 2002. The neuropathological and behavioral consequences of intraspinal microglial/macrophage activation. J Neuropathol Exp Neurol 61:623–633.

Porta C, Rimoldi M, Raes G, Brys L, Ghezzi P, Di Liberto D, Dieli F, Ghisletti S, Natoli G, De Baetselier P, Mantovani A, Sica A. 2009. Tolerance and M2 (alternative) macrophage polarization are related processes orchestrated by p50 nuclear factor kappaB. Proc Natl Acad Sci U S A 106:14978–14983.

Rapalino O, Lazarov-Spiegler O, Agranov E, Velan GJ, Yoles E, Fraidakis M, Solomon A, Gepstein R, Katz A, Belkin M, Hadani M, Schwartz M. 1998. Implantation of stimulated homologous macrophages results in partial recovery of paraplegic rats. Nat Med 4:814–821.

Rolls A, Shechter R, Schwartz M. 2009. The bright side of the glial scar in CNS repair. Nat Rev Neurosci 10:235–241.

Rosenzweig HL, Lessov NS, Henshall DC, Minami M, Simon RP, Stenzel-Poore MP. 2004. Endotoxin preconditioning prevents cellular inflammatory response during ischemic neuroprotection in mice. Stroke 35:2576–2581.

Samanta M, Iwakiri D, Takada K. 2008. Epstein-Barr virus-encoded small RNA induces IL-10 through RIG-I-mediated IRF-3 signaling. Oncogene 27:4150–4160.

Shen Q, Goderie SK, Jin L, Karanth N, Sun Y, Abramova N, Vincent P, Pumiglia K, Temple S. 2004. Endothelial cells stimulate self-renewal and expand neurogenesis of neural stem cells. Science 304:1338–1340.

Singh AK, Jiang Y. 2004. How does peripheral lipopolysaccharide induce gene expression in the brain of rats? Toxicology 201:197–207.

Stevens SL, Leung PY, Vartanian KB, Gopalan B, Yang T, Simon RP, Stenzel-Poore MP. 2011. Multiple preconditioning paradigms converge on interferon regulatory factor-dependent signaling to promote tolerance to ischemic brain injury. J Neurosc i31:8456–8463.

Stirling DP, Yong VW. 2008. Dynamics of the inflammatory response after murine spinal cord injury revealed by flow cytometry. J Neurosci Res 86:1944–1958.

Tasaki K, Ruetzler CA, Ohtsuki T, Martin D, Nawashiro H, Hallenbeck JM. 1997. Lipopolysaccharide pretreatment induces resistance against subsequent focal cerebral ischemic damage in spontaneously hypertensive rats. Brain Res 748:267–270.

Thompson CD, Zurko JC, Hanna BF, Hellenbrand DJ, Hanna A. 2013. The therapeutic role of interleukin-10 after spinal cord injury. J Neurotrauma 30:1311–1324.

van der Poll T, Marchant A, Keogh CV, Goldman M, Lowry SF. 1996. Interleukin-10 impairs host defense in murine pneumococcal pneumonia. J Infect Dis 174:994–1000.

Vartanian KB, Stevens SL, Marsh BJ, Williams-Karnesky R, Lessov NS, Stenzel-Poore MP. 2011. LPS preconditioning redirects TLR signaling following stroke: TRIF-IRF3 plays a seminal role in mediating tolerance to ischemic injury. J Neuroinflamm 8:140.

Yamamoto M, Sato S, Hemmi H, Hoshino K, Kaisho T, Sanjo H, Takeuchi O, Sugiyama M, Okabe M, Takeda K, Akira S. 2003. Role of adaptor TRIF in the MyD88-independent toll-like receptor signaling pathway. Science 301:640–643.

Zhang YK, Liu JT, Peng ZW, Fan H, Yao AH, Cheng P, Liu L, Ju G, Kuang F. 2013. Different TLR4 expression and microglia/macrophage activation induced by hemorrhage in the rat spinal cord after compressive injury. J Neuroinflamm 10:112.

Japan College of Rheumatology
MODERN RHEUMATOLOGY

http://informahealthcare.com/mor
ISSN 1439-7595 (print), 1439-7609 (online)

Mod Rheumatol, 2015; 25(2): 286–291

DOI: 10.3109/14397595.2014.941438

informa
healthcare

ORIGINAL ARTICLE

Clinical and radiographic outcomes of total hip replacement with poly(2-methacryloyloxyethyl phosphorylcholine)-grafted highly cross-linked polyethylene liners: Three-year results of a prospective consecutive series

Yoshio Takatori[1], Toru Moro[1,2], Kazuhiko Ishihara[3], Morihide Kamogawa[4], Hiromi Oda[5], Takashige Umeyama[6], Yoon Taek Kim[5], Hideya Ito[2,7], Masayuki Kyomoto[1,3,8], Takeyuki Tanaka[2], Hiroshi Kawaguchi[2], and Sakae Tanaka[2]

[1]*Division of Science for Joint Reconstruction, Graduate School of Medicine, The University of Tokyo, Tokyo, Japan,* [2]*Orthopaedic Surgery, Sensory and Motor System Medicine, Surgical Sciences, Graduate School of Medicine, The University of Tokyo, Tokyo, Japan,* [3]*Department of Materials Engineering, School of Engineering, The University of Tokyo, Tokyo, Japan,* [4]*Department of Orthopaedic Surgery, JR Tokyo General Hospital, Tokyo, Japan,* [5]*Department of Orthopaedic Surgery, Saitama Medical University School of Medicine, Saitama, Japan,* [6]*Department of Orthopedic Surgery, NTT Medical Center Tokyo, Tokyo, Japan,* [7]*Department of Orthopaedic Surgery, Japan Red Cross Medical Center, Tokyo, Japan, and* [8]*Research Department, KYOCERA Medical Corporation, Osaka, Japan*

Abstract

Objectives. This study aimed to evaluate the clinical safety and wear-resistance of the novel highly cross-linked polyethylene (HXLPE) acetabular liner with surface grafting of poly(2-methacryloyloxyethyl phosphorylcholine) (PMPC) at 3 years after total hip replacement (THR).

Methods. Eighty consecutive patients underwent cementless THR using a 26-mm diameter cobalt–chromium–molybdenum alloy femoral head and a PMPC-grafted HXLPE liner for the bearing couplings. We evaluated the clinical and radiographic outcomes of 76 patients at 3 years after the index surgery.

Results. The clinical results at 3 years were equivalent to a Harris hip score of 95.6 points. No adverse events were associated with the implanted PMPC-grafted HXLPE liner, and no periprosthetic osteolysis was detected. The mean femoral head penetration rate was 0.002 mm/year, representing marked reduction compared with other HXLPE liners.

Conclusions. A PMPC-grafted HXLPE liner is a safe option in THR and probably reduces the generation of wear particles.

Keywords

Arthroplasty, Hip prosthesis, Joint replacement, Polyethylene (UHMWPE), Wear

History

Received 26 March 2014
Accepted 18 June 2014
Published online 12 August 2014

Introduction

Total hip replacement (THR) is an established treatment modality for patients with end-stage hip disorders such as osteoarthritis and rheumatoid arthritis. However, periprosthetic osteolysis has been recognized as a notable complication affecting the long-term survival of THR; extensive research has shown that wear particles from the polyethylene (PE) liners are responsible for osteolysis [1]. Hence, many approaches have been adopted for reducing the generation of wear particles thereby improving the survival of THR.

Recent observations of the healthy mammalian articular cartilage surface have disclosed that it is covered with a nanometer-scaled phospholipid layer that protects the articulating surface from mechanical wear and facilitates a smooth motion of joints during daily activities [2,3]. Hence, grafting a polymer with a phospholipid-like layer on the liner surface may mimic the surface conditions of healthy articular cartilage. Based on this hypothesis, we have successfully produced a biocompatible and highly hydrophilic surface via nanometer-scaled grafting of poly(2-methacryloyloxyethyl phosphorylcholine) (PMPC) onto highly cross-linked polyethylene (HXLPE) [4]. Our hip simulator studies revealed that such grafting remarkably reduced the wear of an HXLPE liner up to 20×10^6 cycles [5–7]. We reported that PMPC-grafted surfaces captured water molecules and reduced the friction between the bearing surfaces via the hydration lubrication mechanism [8]. In addition, we reported that the PMPC-grafted particles were biologically inert and did not cause subsequent bone-resorptive responses [4], indicating that this technology prevents wear particle production and biological reactions to such particles in THR. Since then, PMPC-grafted HXLPE liners have been used in hip replacement surgery to address the concerns of wear and osteolysis.

From the perspective of material engineering, the PMPC-grafted HXLPE liner is a new medical implant prepared from MPC polymer, which has been used on the surface of artificial lungs [9], intravascular stents [10], soft contact lenses [11], and the artificial hearts [12]. Such implants were introduced into clinical practice from 1997, and since then, no adverse reactions to MPC polymer have been reported. The major difference between other devices and the PMPC-grafted HXLPE liner is the method used for its MPC polymer coating, the photo-induced graft polymerization, which is considered appropriate for withstanding weight [4].

Correspondence to: Toru Moro, Division of Science for Joint Reconstruction, Graduate School of Medicine, The University of Tokyo, 7-3-1 Hongo, Bunkyo-ku, Tokyo 113-8655, Japan. Tel: +81-3-5800-8656. Fax: +81-3-3818-4082. E-mail: moro-ort@h.u-tokyo.ac.jp

The purpose of this follow-up for a prospective cohort study, in which 80 primary cementless THRs were performed using a PMPC-grafted HXLPE liner [13], was to report the clinical and radiographic outcomes, including femoral head penetration, at 3 years after the index surgery. The outline of this study was disclosed as UMIN000003681.

Methods

Between April 2007 and September 2008, 80 consecutive patients who underwent THR for a Charnley Class A or Class B painful, non-infectious hip disorder were recruited from five participating hospitals [14]. The institutional review board of each participating hospital granted ethical approval, and informed consent was obtained from all participants before the study commenced.

All patients received the K-MAX cementless THR (KYOCERA Medical Corporation, Osaka, Japan) consisting of a collarless femoral stem (K-MAX HS-6) and a low-profile porous-coated acetabular component with four peripheral fins (K-MAX Q5LP). For the bearing coupling, a 26-mm-diameter cobalt–chromium–molybdenum (Co–Cr–Mo) alloy femoral head and a PMPC-grafted HXLPE liner were employed. PMPC grafting of the surfaces of the HXLPE liner was performed using a photoinduced polymerization technique as previously reported [4].

The surgeries were performed by 10 surgeons of 5 institutions, who used the posterior approach. Patients underwent the routine thromboprophylaxis regimen and postoperative rehabilitation program of each institution.

All patients were prospectively followed for 3 years after the index surgery. During the course of the study, all adverse events suspected to correlate with the implanted PMPC-grafted HXLPE liner were recorded. Orthopedic surgeons other than the operators evaluated clinical performance using the evaluation chart of hip joint function authorized by the Japanese Orthopaedic Association (JOA score) [15]. The JOA score consists of four categories: pain (40 points), range of motion (20 points), gait (20 points), and activities of daily living (20 points). Fujisawa et al. reported that there was an excellent correlation between the JOA and Harris hip scores (coefficient of correlation = 0.843) [16]. Therefore, we calculated the equivalent Harris hip score using the following regression formula: Harris hip score = JOA score × 0.979 + 4.363.

Anteroposterior pelvic radiographs were obtained with the patient in supine, immediately after surgery and at 3 weeks, 3 months, 6 months, 1 year, and 3 years postoperatively. The distance between the X-ray tube and the imaging plate was set to 100 cm, and the center of the X-ray beam was directed at the cranial end of the pubic symphysis. The digitized image data were stored at a resolution of 0.13–0.20 mm/pixel.

We compared the radiographs obtained at 3 weeks with those obtained at up to 3 years for detecting periprosthetic osteolysis and assessing implant stability. Periprosthetic osteolysis was defined as new cystic lucency localized on the endosteal surface of the bone [17]. Migration of the femoral component was defined as a change of 3 mm or above in the position of the implant [18]. To assess the stability of the acetabular component, we modified the method described by Engh et al. [19]. The acetabular component was defined as stable, suboptimally stable (migrated ≤2 mm or tilted ≤5°), or unstable (migrated >2 mm or tilted >5°).

In addition, three independent reviewers measured the position of the femoral head on digitized radiographic images obtained at 3 weeks, 6 months, 1 year, and 3 years after implantation, without any clinical information. They employed a 2D computerized method—the PolyWare technique (Draftware Inc., Vevay, IN) [20]. Each reviewer measured the position of the femoral head thrice on a radiograph and recorded the median as the measured value. The authors calculated the average value of the three measured values recorded by the three reviewers and stored it in a database as the observed data. Then, they calculated the change in the femoral head position in each patient as the amount of femoral head penetration using the position at 3 weeks as the original position.

Several authors have reported a biphasic pattern in the progression of femoral head penetration into an HXLPE liner [19,21–25]. In the first phase, the femoral head rapidly moves into the liner; this phenomenon is called "bedding-in" and is largely attributed to permanent plastic deformation of the material and setting of the liner in the metal shell [22]. In the second phase, the femoral head slowly moves into the liner; this phenomenon is largely attributed to true wear—material loss in the form of particles—and is considered the "steady-state wear rate". We used these terms to describe the measurement results.

Statistical methods

The paired t-test was used to compare the JOA scores recorded before surgery and at 3 years after surgery. Pearson's correlation coefficient or the Mann–Whitney *U* test was employed to test the correlations between the measurement of femoral head penetration and patient characteristics, such as body mass index (BMI).

Results

Of the original 80 patients, 1 died of a cause unrelated to the joint replacement and 3 were lost or refused to return for follow-up at 3 years postoperatively. Thus, the study group comprised 76 patients (Table 1).

No adverse events suspected to correlate with the implanted PMPC-grafted HXLPE liner were recorded, and no revision

Table 1. Preoperative demographic data.

Items	Patients (%)
All patients	76
Sex	
Male	14 (18.4)
Female	62 (81.6)
Age (years)	
40–49	5 (6.6)
50–59	30 (39.5)
60–69	22 (28.9)
70–75	19 (25.0)
Diagnosis	
Osteoarthritis	73 (96.1)
Osteonecrosis	3 (3.9)
Charnley Category	
A	40 (52.6)
B	36 (47.4)
Side	
Right	42 (55.3)
Left	34 (44.7)
Body Height (cm)	
>140 to ≦150	17 (22.4)
>150 to ≦160	40 (52.6)
>160 to ≦170	18 (23.7)
>170 to ≦180	1 (1.3)
Mean ± SD	155.5 ± 6.5
Body Weight (kg)	
>30 to ≦40	4 (5.3)
>40 to ≦50	17 (22.4)
>50 to ≦60	41 (53.9)
>60 to ≦70	13 (17.1)
>70 to ≦80	1 (1.3)
Mean ± SD	54.4 ± 7.4
Body Mass Index	
>15 to ≦20	11 (14.5)
>20 to ≦25	49 (64.5)
>25 to ≦30	16 (21.1)
Mean ± SD	22.5 ± 2.5

Mod Rheumatol, 2015; 25(2): 286–291

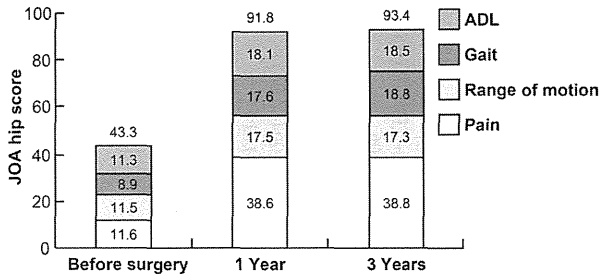

Figure 1. Average Japanese Orthopaedic Association hip score before surgery and at 1 and 3 years after surgery. The change was most apparent in the pain category.

operations were performed during the follow-up period. Three patients had deep vein thrombosis, which was treated successfully with anticoagulants in each case. Two patients had dislocation, which was treated nonoperatively and no deep infection occurred.

The mean JOA score improved at 3 years postoperatively ($p < 0.01$; Figure 1). According to Fujisawa's regression formula [16], the mean JOA score immediately after THR and at 3 years after THR corresponded with Harris hip scores of 46.7 and 95.6, respectively. Therefore, the clinical outcomes of the present cohort were similar to those of other contemporary cementless THRs [22,24].

On radiographic analysis, neither periprosthetic osteolysis nor femoral component migration was detected in all 76 patients (Figure 2). Seventy-four patients had a stable acetabular component and two had a suboptimally stable component. In the two patients with a suboptimally stable acetabular component, the component had changed its position up to 6 months after the index surgery and was stable afterwards. Similar observations have been reported in other cementless acetabular components and are not compatible with the predictive radiographic findings for the early diagnosis of loosening [19,26]. We attributed this limited migration to insufficient initial seating of the component.

Penetration during the first year was regarded as bedding-in and that after 1 year as steady-state wear [21,25]. Among all patients, 38 (50%) had negative wear between 1 and 3 years. The mean femoral head penetration rate between 1 and 3 years was 0.002 mm/year (Figure 3), representing marked reduction compared with the mean wear rate of other HXLPE liners [19,21–25]. The mean femoral head penetration rate correlated weakly with patient age ($R = 0.331$), but it did not correlate with sex, preoperative diagnosis, body weight, or BMI.

In the present cohort, the mean penetration at 1 year was 0.210 mm, and was slightly greater in male patients than that in female

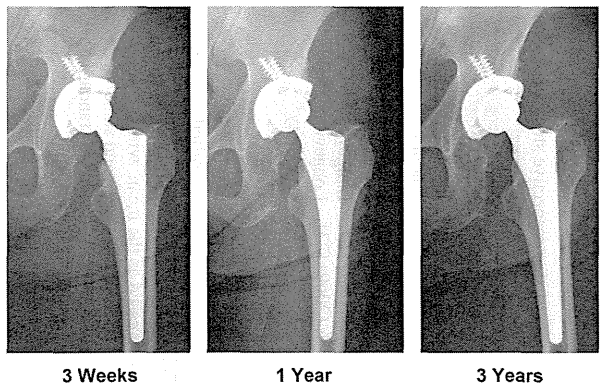

Figure 2. Radiographs of a representative case (Case 66). Radiographs obtained 3 weeks, 1 year, and 3 years after surgery, showing no findings related to implant migration or periprosthetic osteolysis.

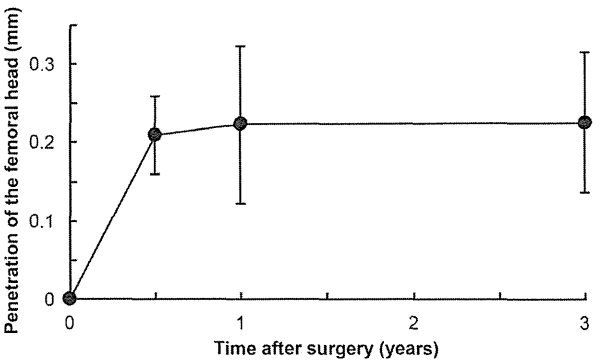

Figure 3. Femoral head penetration at 6 months, 1 year, and 3 years after surgery. The amount of femoral head penetration is calculated using the position at 3 weeks as the original position. Penetration during the first year is larger than that in the subsequent 2 years. Standard deviation bars are displayed.

patients ($p = 0.021$). Although men were heavier than women ($p = 0.014$), the mean penetration did not correlate with body weight. We also found no correlation between mean penetration at 1 year and patient age, preoperative diagnosis, and BMI. Mean penetration at 3 years correlated weakly with BMI (Figure 4), but it did not correlate with sex, age, preoperative diagnosis, or body weight.

We compared the data of the 2 patients with a suboptimally stable acetabular component with those of the 74 patients with a stable component (Table 2). In one patient (Case 33), a large amount of penetration was observed at 6 months, and the value decreased up to 3 years after surgery. In the other patient (Case 36), the amount of penetration was relatively small at 1 year and relatively large at 3 years. As a result, this patient showed a high wear rate between 1 and 3 years. The cause of these unusual observations is unclear and continued follow-up is required to determine their relevance to the clinical outcome.

Discussion

To support the continued use of a new implant, updated clinical data should be available on the safety and efficacy. PMPC-grafted HXLPE liners were introduced to address concerns of wear and osteolysis in hip replacement. Regarding the safety of these implants, this study demonstrated that THR using this liner provided good clinical results, and no adverse events associated with the liner occurred during the 3 years after implantation. Therefore, this liner should be considered as a safe option in hip replacement.

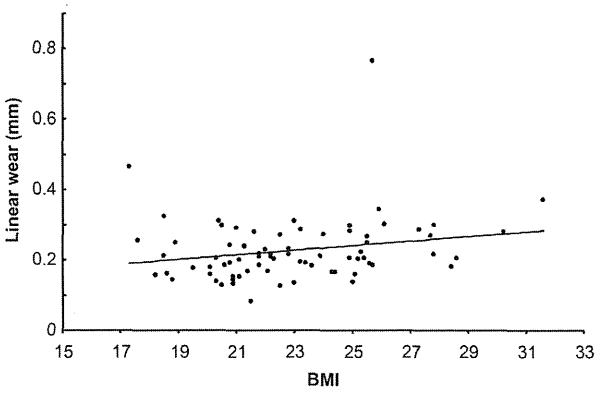

Figure 4. Relationship between amount of femoral head penetration at 3 years after surgery and body mass index. $y = 0.0065x + 0.077$; $R = 0.215$.

Table 2. Summary of the results of measurement of the penetration of the femoral heads.

	All hips (76 hips)*	Stable (74 hips)*	Suboptimally stable (2 hips)	
			Case 33	Case 36
6 months (mm)	0.210 ± 0.050	0.196 ± 0.050	1.050	0.170
1 year (mm)	0.223 ± 0.100	0.214 ± 0.069	0.863	0.137
3 years (mm)	0.226 ± 0.090	0.218 ± 0.065	0.765	0.302
Wear rate (mm/year)	0.002 ± 0.043	0.002 ± 0.041	− 0.049	0.083

*Values are expressed as mean and standard deviation.

Regarding the efficacy of PMPC-grafting in reducing wear, the mean amount of bedding-in was 0.210 mm and the steady-state wear rate was 0.002 mm/year in the present study. We found no osteolysis on serial radiographs. For comparison, the results of six other prospective studies are summarized in Table 3 [19,21–25]. In these studies, a 26- or 28-mm-diameter Co–Cr–Mo alloy femoral head and HXLPE liner secured in a cementless shell were used for the bearing coupling, and the patients were followed for at least 3 years. Among these studies, three reported detailed data on bedding-in: it occurred from 6 months to 1 year after surgery, and the mean amount of penetration ranged from 0.123 to 0.260 mm. Thus, in the first year, the behavior of the PMPC-grafted HXLPE liner is quite similar to that of other liners. Because PMPC grafting is nanometer-scaled surface modification, this technique does not affect the physical or mechanical properties of the HXLPE substrate [27]. Hence, we attributed the differences in the amount of penetration to the characteristics of the HXLPE liners. They can vary in terms of resin type, radiation technique used for cross-linking, post-irradiation stabilization process, and sterilization modality, any of which can influence the mechanical properties, crystallinity, and pre-aging and post-aging oxidation levels of the components [28]. For instance, Medel et al. reported that annealing preserves the mechanical properties better than remelting with regard to both fatigue and fracture resistance [29]. Meanwhile, all six studies reported steady-state penetration rates: they varied from 0.01 to 0.06 mm/year. Although PE wear is a multifactorial process [18], the results of the present study seem to compare favorably with those of the other six studies in terms of marked reduction. Among patient characteristics, the body weight of the patients was significantly lesser in the present study than in the other studies. Therefore, we believe that PMPC grafting is a promising method for reducing HXLPE wear, and the results of the present study support the continued use of these liners. We plan to conduct a longer follow-up to elucidate the true clinical benefit of PMPC-grafted HXLPE liners in hip replacement surgery.

This study has several limitations. First, it was not a randomized controlled trial. A randomized controlled trial comparing HXLPE liners and PMPC-grafted HXLPE liners would be the best scientific method to evaluate the efficacy of PMPC grafting. However, most candidates reported that they preferred the new liner and did not want to join a clinical trial in which their liner was chosen by a chance mechanism. Therefore, we performed a prospective cohort study to address this issue.

Second, 76 individuals and a 3-year follow-up may not be sufficient to deny the possibility of rare adverse reactions related to these new bearings. Thus, a long-term follow-up study (UMIN000003681) is underway for an extended investigation.

Third, the radiostereometric analysis (RSA) method, which has been reported to be the most accurate tool for in vivo assessment of PE wear [30], was not used in this study because of the need for the placement of marker balls. Many potential candidates believed that these metals provided no benefit. Therefore,

Table 3. Summary of six prospective studies using a 26- or 28-mm cobalt–chromium–molybdenum alloy femoral head with highly cross-linked polyethylene liner.

Authors	HXLPE	Head size (mm)	n	Body weight (kg)	BMI	Follow-up (year)*	Measurement technique	Bedding-in duration (year)	Amount of Bedding-in (mm)†	Steady-state penetration rate (mm/y)‡
Engh et al. (2006) [19]	Marathon®	28	76	84.4 ± 21.3 (51.3–149.4)	28.6 ± 5.5 (19.9–47.3)	5.5 (4.1–7.0)	Hip Analysis Suite	0.75 ≦	0.22 ± 0.31	0.01 ± 0.07
Calvert et al. (2009) [22]	Marathon®	28	59	NA	NA	4	PolyWare Auto	0.5	NA	0.0239 (−0.008–0.0558)
Glyn-Jones et al. (2008) [21]	Longevity®	28	26	79 (49–117)	NA	3	RSA	1	0.26 ± 0.17	0.03 ± 0.06
Lachiewicz et al. (2009) [23]	Longevity®	26	14	NA	29 (18.9–46.4)	5.7 (5–8)	Hip Analysis Suite	NA	NA	0.060 ± 0.042
Lachiewicz et al. (2009) [23]	Longevity®	28	33	NA	29 (18.9–46.4)	5.7 (5–8)	Hip Analysis Suite	NA	NA	0.032 ± 0.019
Whittaker et al. (2010) [24]	Longevity®	28	36	78.9 ± 13.8	29.3 ± 3.9	7.64 (6.60–8.53)	Hip Analysis Suite	NA	NA	0.025 (0.009–0.042)
Whittaker et al. (2010) [24]	XLPE®	28	47	88.7 ± 23.4	31.1 ± 6.3	6.42 (5.0–8.01)	Hip Analysis Suite	NA	NA	0.026 (0.004–0.047)
Capello et al. (2011) [25]	Crossfire®	28	42	79.2 ± 19.6	27.4 ± 4.5	8.6 (7.0–10.3)	Livermore	1	0.123	0.031 ± 0.014
Present study	Poly(MPC)-grafted	26	76	55.1 ± 8.2 (37.0–77.9)	22.9 ± 3.0 (17.3–31.6)	3	PolyWare	1	0.223 ± 0.100	0.002 ± 0.043

HXLPE highly cross-linked polyethylene, *NA* not available
*Values are expressed as the mean, with the range in parentheses.
†Values are expressed as the mean and standard deviation.
‡Values are expressed as the mean and standard deviation, or 95% confidence limit in parentheses.

we employed the PolyWare technique instead. As reported by Stilling et al., mean PE wear measured with PolyWare tends to be greater than that measured using the RSA method [31]. Consequently, the present study possibly overestimated the amount of penetration.

Fourth, among all patients, 38 (50%) had negative wear between 1 and 3 years. Such results are common in short-term studies of HXLPE liners [19,23,24]. Engh et al. reported a negative wear rate in 32% of the patients in their study [19]. As Lachiewicz et al. pointed out, these paradoxical observations should be attributed to the detection limits of the measurement technique [23].

Fifth, we used 26-mm-diameter Co–Cr–Mo alloy heads on the femoral side. However, in the clinical setting, various femoral heads of larger sizes and materials are available. Although we confirmed that improvements due to PMPC grafting surpassed those due to changes in the femoral head sizes or materials in the hip joint simulator studies [32], the outcome of THR using other femoral heads should be evaluated to determine the clinical utility of PMPC-grafted HXLPE liners. A multicenter study (UMIN000008730) is currently underway for the evaluation of other femoral heads, including zirconia-toughened alumina ceramic femoral heads and femoral heads with a larger diameter [33].

In conclusion, this study demonstrated that use of a PMPC-grafted HXLPE liner in THR appears to provide good clinical and radiographic results at 3 years after the index surgery. Further follow-up is needed to determine whether PMPC-grafted HXLPE liners improve long-term clinical outcomes.

Acknowledgments

The authors would like to thank the late Dr. Shuhei Morimoto for his invaluable contribution and participation in the present study since 2006.

Conflict of interest

One or more of the authors or institutions received outside funding or grants from KYOCERA Medical Corporation. One of the authors (K.M.) is employed by KYOCERA Medical Corporation.

References

1. Willert HG, Bertram H, Buchhorn GH. Osteolysis in alloarthroplasty of the hip. The role of ultra-high molecular weight polyethylene wear particles. Clin Orthop Relat Res. 1990;258:95–107.
2. Kirk TB, Wilson AS, Stachowiak GW. The morphology and composition of the superficial zone of mammalian articular cartilage. J Orthop Rheumatol. 1993;6:21–8.
3. Hills BA. Boundary lubrication in vivo. Proc Inst Mech Eng [H]. 2000;214:83–94.
4. Moro T, Takatori Y, Ishihara K, Konno T, Takigawa Y, Matsushita T, et al. Surface grafting of artificial joints with a biocompatible polymer for preventing periprosthetic osteolysis. Nat Mater. 2004;3(11): 829–36.
5. Moro T, Takatori Y, Ishihara K, Nakamura K, Kawaguchi H. Grafting of biocompatible polymer for longevity of artificial hip joints. Clin Orthop Relat Res. 2006;453:58–63.
6. Moro T, Kyomoto M, Ishihara K, Saiga K, Hashimoto M, Tanaka S, et al. Grafting of poly (2-methacryloyloxyethyl phosphorylcholine) on polyethylene liner in artificial hip joints reduces production of wear particles. J Mechan Behav Biomed Mater. 2014;31:100–6.
7. Moro T, Takatori Y, Kyomoto M, Ishihara K, Hashimoto M, Ito H, et al. Long-term hip simulator testing of the artificial hip joint bearing surface grafted with biocompatible phospholipid polymer. J Orthop Res. 2014;32(3):369–76.
8. Kyomoto M, Moro T, Saiga K, Hashimoto M, Ito H, Kawaguchi H, et al. Biomimetic hydration lubrication with various polyelectrolyte layers on cross-linked polyethylene orthopedic bearing materials. Biomaterials. 2012;33(18):4451–9.
9. Myers GJ, Johnstone DR, Swyer WJ, McTeer S, Maxwell SL, Squires C, et al. Evaluation of Mimesys phosphorylcholine (PC)-coated oxygenators during cardiopulmonary bypass in adults. J Extra Corpor Technol. 2003;35(1):6–12.
10. Kuiper KK, Nordrehaug JE. Early mobilization after protamine reversal of heparin following implantation of phosphorylcholine-coated stents in totally occluded coronary arteries. Am J Cardiol. 2000;85(6):698–702.
11. Selan L, Palma S, Scoarughi GL, Papa R, Veeh R, Di Clemente D, Artini M. Phosphorylcholine impairs susceptibility to biofilm formation of hydrogel contact lenses. Am J Ophthalmol. 2009; 147(1):134–9.
12. Snyder TA, Tsukui H, Kihara S, Akimoto T, Litwak KN, Kameneva MV, et al. Preclinical biocompatibility assessment of the EVAHEART ventricular assist device: Coating comparison and platelet activation. J Biomed Mater Res A. 2007;81(1):85–92.
13. Takatori Y, Moro T, Kamogawa M, Oda H, Morimoto S, Umeyama T, et al. Poly(2-methacryloyloxyethyl phosphorylcholine)-grafted highly cross-linked polyethylene liner in primary total hip replacement: one-year results of a prospective cohort study. J Artif Organs. 2013;16(2):170–5.
14. Charnley J. The long-term results of low-friction arthroplasty of the hip performed as a primary intervention. J Bone Joint Surg Br. 1972;54(1):61–76.
15. Imura S. Evaluation chart of hip join functions. J Jpn Orthop Assoc. 1995;69:860–7.
16. Fujisawa M, Naito M, Asayama I. A comparative study of hip joint functional scoring systems between Japanese Orthopaedic Association hip score and Harris hip score. Seikeigeka. 2001;52: 628–33 (in Japanese).
17. Nagai I, Takatori Y, Kuruta Y, Moro T, Karita T, Mabuchi A, Nakamura K. Nonself-centering Bateman bipolar endoprosthesis for nontraumatic osteonecrosis of the femoral head: a 12- to 18-year follow-up study. J Orthop Sci. 2002;7(1):74–8.
18. Sutherland CJ, Wilde AH, Borden LS, Marks KE. A ten-year follow-up of one hundred consecutive Müller curved-stem total hip-replacement arthroplasties. J Bone Joint Surg Am. 1982;64(7):970–82.
19. Engh CA Jr, Stepniewski AS, Ginn SD, Beykirch SE, Sychterz-Terefenko CJ, Hopper RH Jr, Engh CA. A randomized prospective evaluation of outcomes after total hip arthroplasty using cross-linked marathon and non-cross-linked Enduron polyethylene liners. J Arthroplasty. 2006;21(Suppl 2):17–25.
20. Hui AJ, McCalden RW, Martell JM, MacDonald SJ, Bourne RB, Rorabeck CH. Validation of two and three-dimensional radiographic techniques for measuring polyethylene wear after total hip arthroplasty. J Bone Joint Surg Am. 2003;85(3):505–11.
21. Glyn-Jones S, McLardy-Smith P, Gill HS, Murray DW. The creep and wear of highly cross-linked polyethylene: a three-year randomised, controlled trial using radiostereometric analysis. J Bone Joint Surg Br. 2008;90(5):556–61.
22. Calvert GT, Devane PA, Fielden J, Adams K, Horne JG. A double-blind, prospective, randomized controlled trial comparing highly cross-linked and conventional polyethylene in primary total hip arthroplasty. J Arthroplasty. 2009;24(4):505–10.
23. Lachiewicz PF, Heckman DS, Soileau ES, Mangla J, Martell JM. Femoral head size and wear of highly cross-linked polyethylene at 5 to 8 years. Clin Orthop Relat Res. 2009;467(12):3290–6.
24. Whittaker JP, Charron KD, McCalden RW, Macdonald SJ, Bourne RB. Comparison of steady state femoral head penetration rates between two highly cross-linked polyethylenes in total hip arthroplasty. J Arthroplasty. 2010;25(5):680–6.
25. Capello WN, D'Antonio JA, Ramakrishnan R, Naughton M. Continued improved wear with an annealed highly cross-linked polyethylene. Clin Orthop Relat Res. 2011;469(3):825–30.
26. Udomkiat P, Wan Z, Dorr LD. Comparison of preoperative radiographs and intraoperative findings of fixation of hemispheric porous-coated sockets. J Bone Joint Surg Am. 2001;83A(12):1865–70.
27. Kyomoto M, Moro T, Konno T, Takadama H, Kawaguchi H, Takatori Y, et al. Effects of photo-induced graft polymerization of 2-methacryloyloxyethyl phosphorylcholine on physical properties of cross-linked polyethylene in artificial hip joints. J Mater Sci Mater Med. 2007;18(9):1809–15.
28. Collier JP, Currier BH, Kennedy FE, Currier JH, Timmins GS, Jackson SK, Brewer RL. Comparison of cross-linked polyethylene materials for orthopaedic applications. Clin Orthop Relat Res. 2003;414:289–304.
29. Medel FJ, Peña P, Cegoñino J, Gómez-Barrena E, Puértolas JA. Comparative fatigue behavior and toughness of remelted and annealed

highly crosslinked polyethylenes. J Biomed Mater Res B Appl Biomater. 2007;83(2):380–90.
30. Kärrholm J, Herberts P, Hultmark P, Malchau H, Nivbrant B, Thanner J. Radiostereometry of hip prostheses. Review of methodology and clinical results. Clin Orthop Relat Res. 1997;344:94–110.
31. Stilling M, Larsen K, Andersen NT, Søballe K, Kold S, Rahbek O. The final follow-up plain radiograph is sufficient for clinical evaluation of polyethylene wear in total hip arthroplasty. A study of validity and reliability. Acta Orthop. 2010;81(5):570–8.
32. Moro T, Kawaguchi H, Ishihara K, Kyomoto M, Karita T, Ito H, et al. Wear resistance of artificial hip joints with poly(2-methacryloyloxyethyl phosphorylcholine) grafted polyethylene: Comparisons with the effect of polyethylene cross-linking and ceramic femoral heads. Biomaterials. 2009;30(16):2995–3001.
33. Kurtz SM, Kocagöz S, Arnholt C, Huet R, Ueno M, Walter WL. Advances in zirconia toughened alumina biomaterials for total joint replacement. J Mech Behav Biomed Mater. 2014; 31:107–16.

J Neurosurg Spine 21:773–777, 2014

Progression of ossification of the posterior longitudinal ligament of the thoracic spine following posterior decompression and stabilization

Clinical article

Shurei Sugita, M.D.,[1] Hirotaka Chikuda, M.D., Ph.D.,[1] Katsushi Takeshita, M.D., Ph.D.,[1] Atsushi Seichi, M.D., Ph.D.,[2] and Sakae Tanaka, M.D., Ph.D.[1]

[1]Department of Orthopaedic Surgery, Faculty of Medicine, University of Tokyo, Tokyo; and [2]Department of Orthopedics, Jichi Medical University, Tochigi, Japan

Object. Despite its potential clinical impact, information regarding progression of thoracic ossification of the posterior longitudinal ligament (OPLL) is scarce. Posterior decompression with stabilization is currently the primary surgical treatment for symptomatic thoracic OPLL; however, it remains unclear whether thoracic OPLL increases in size following spinal stabilization. It is also unknown whether patients' clinical symptoms worsen as OPLL size increases. In this retrospective case series study, the authors examined the postoperative progression of thoracic OPLL.

Methods. Nine consecutive patients with thoracic OPLL who underwent posterior decompression and fixation with a minimum follow-up of 3 years were included in this study. Thin-slice CT scans of the thoracic spine obtained at the time of surgery and the most recent follow-up were analyzed. The level of the most obvious protrusion of ossification was determined using the sagittal reconstructions, and the ossified area was measured on the axial reconstructed scan at the level of the most obvious protrusion of ossification using the DICOM (digital imaging and communications in medicine) software program. Myelopathy severity was assessed according to the Japanese Orthopaedic Association (JOA) scale score for lower-limb motor function on admission, at postoperative discharge, and at the last follow-up visit.

Results. The OPLL area was increased in all patients. The mean area of ossification increased from 83.6 ± 25.3 mm^2 at the time of surgery to 114.8 ± 32.4 mm^2 at the last follow-up visit. No patients exhibited any neurological deterioration due to OPLL progression.

Conclusions. The present study demonstrated that the size of the thoracic OPLL increased after spinal stabilization. Despite diminished local spinal motion, OPLL progression did not decrease or stop. Physicians should pay attention to ossification progression in patients with thoracic OPLL.

(http://thejns.org/doi/abs/10.3171/2014.7.SPINE131191)

Key Words • **posterior decompression and fixation** • **thoracic spine** • **ossification of the posterior longitudinal ligament** • **progression**

Ossification of the posterior longitudinal ligament (OPLL) is a condition of the spine characterized by the ectopic ossification of the spinal ligaments, potentially resulting in myelopathy due to spinal cord compression.[11] Although cervical OPLL progression is well documented in the literature,[1,7,14,17,18] information regarding thoracic OPLL progression is lacking. Currently, posterior decompression and stabilization using instrumentation is a widely used first-choice treatment for symptomatic thoracic OPLL and achieves good short-term outcomes.[8,9,12,20] Anterior decompression is technically demanding, and the technique is associated with a high rate of complications.[13,16] Spinal fixation with instrumentation is believed to diminish spinal cord damage and suppress further ossification by eliminating dynamic effects and reducing mechanical stress.[19] Although the long-term progression of OPLL may compromise the surgical benefits, it remains unclear whether thoracic OPLL continues to grow after spinal stabilization. We hypothesized that spinal stabilization decreases the rate of OPLL progression by immobilizing the spine. To address this

Abbreviations used in this paper: JOA = Japanese Orthopaedic Association; OPLL = ossification of the posterior longitudinal ligament.

This article contains some figures that are displayed in color online but in black-and-white in the print edition.

issue, we examined thin-slice CT scans of patients with thoracic OPLL who underwent posterior decompression and fixation to examine the postoperative progression of thoracic OPLL.

Methods

Patients

There were 16 patients who underwent surgery for thoracic OPLL in the study period (from 2004 to 2007). Nine consecutive patients with thoracic OPLL who underwent posterior decompression and instrumentation-assisted fixation and had a minimum follow-up period of 3 years were included in this study. Three patients were excluded because they underwent OPLL extirpation via an anterior approach. Another 4 patients were excluded because the follow-up period was shorter than 3 years. All patients presented with progressive gait disturbance. We performed posterior decompression and fixation with a pedicle screw and rod system. The surgical plans were individualized according to OPLL extension and concomitant ossification of the ligamentum flavum. We fixed the spine 2–3 levels above and below the decompression levels and harvested local bone for grafting. In this group, plain radiography did not provide sufficient information regarding the instrumentation failure or ossification progression. Therefore, as part of the standard follow-up protocol, we obtained CT scans of OPLL patients every 2–3 years after surgery. We examined the thin-slice CT images of the thoracic spine obtained at the time of surgery and at the most recent follow-up visit. The CT scans were obtained with a slice thickness of 0.75 mm and a pixel size of 0.352 × 0.352 mm. The data were transferred via a DICOM (digital imaging and communications in medicine) network to a computer workstation using the OsiriX software program (OsiriX Imaging Software).[5] Our institution's ethics board approved the study protocol.

Clinical Data

The patients' medical charts were reviewed for age, sex, type and extension of OPLL, and surgical procedure. Myelopathy severity was assessed according to the Japanese Orthopaedic Association (JOA) scale for lower-limb motor function,[8] which was administered on admission, at discharge, and the latest follow-up visit.

Measurement of Ossification

We reconstructed all preoperative CT scans for 3D multiplanar reconstruction and, using the sagittal reconstruction, determined the thoracic spine level with the most obvious level of ossification protrusion. We then measured the area of ossification on the axial reconstruction, which was set parallel to the endplate of the corresponding vertebra, using the OsiriX software program (Fig. 1). We also measured ossification area on the latest follow-up CT scan at the same level. All measurements were obtained twice for each CT data set by a board-certified spine surgeon (author S.S.), and the average value of the 2 measurements was used.

Statistical Analysis

We performed statistical analyses of the data using the Wilcoxon signed-rank test. Differences were considered statistically significant if p values were < 0.05. Mean values are presented ± SD.

Results

Demographic Data

The population included 3 males and 6 females, whose mean age was 56 ± 12.2 years (range 38–75 years). The mean follow-up period was 4.6 ± 2.0 years (range 3–9 years). The type of OPLL was continuous in 3 patients, mixed in 4 patients, and circumscribed in 2 patients. The level of OPLL, the level of the most obvious protrusion, and the surgical areas of decompression and fixation are shown in Table 1.

OPLL Progression

The area of OPLL was found to have increased in all patients (Table 2 and Fig. 2). The average area of ossification was 83.6 ± 25.3 mm^2 preoperatively and 114.8 ±

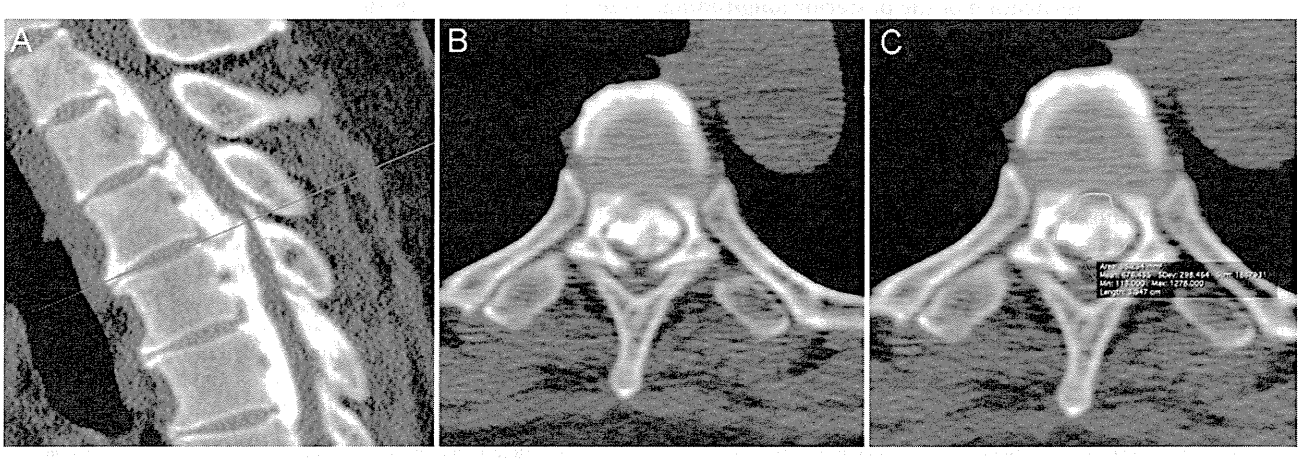

Fig. 1. A: The level of the most obvious protrusion of ossification was determined in the sagittal reconstruction *(line)*. **B:** Cross-section at the determined level. **C:** The area of ossification, shown in *green*, was measured using a software function.

TABLE 1: Patient demographics

Patient No.	Age (yrs), Sex	Type of OPLL	Extension of OPLL		Most Protruded OPLL Level	Surgical Level		Implant Density*	Rod Diameter (mm)	Follow-Up (yrs)
			Preop	Last Follow-Up		Decompression	Fixation			
1	48, M	mixed	C7–T10	C7–T10	T7–8	T1–10	T1–12	0.5	5.5	9
2	58, F	continuous	T3–6	T3–6	T5–6	T1–10	T1–10	0.55	5.5	3
3	38, M	circumscribed	T7–11	T7–11	T8–9	T7–L1	T5–L2	0.75	5.5	4
4	55, F	mixed	T4–10	T4–10	T5–6	T2–12	T2–12	0.55	6.5	3
5	64, F	continuous	T5–10	T3–L1	T7–8	T5–10	T5–10	0.92	5.5	7
6	39, M	circumscribed	T7–8	T7–8	T7–8	T5–10	T5–10	0.67	5.5	5
7	75, F	continuous	T3–9	T1–T11	T8–9	T5–10	T5–10	0.75	5.5	3
8	63, F	mixed	C4–T7	C4–T8	T3–4	C3–T8	C7–T8	0.56	6.5	4
9	70, F	mixed	C7–T5	C6–T5	T–2	C3–T6	C7–T8	0.67	5.5	3

* Implant density = no. implants per fixation segment × 2.

32.4 mm² at the last follow-up visit. All areas of ossification increased in both width and thickness. Longitudinal OPLL progression was also noted in 4 of 9 patients. The rate of OPLL progression (the most recent size before surgery) was not correlated with the rod diameter or implant density. Neither screw loosening nor rod breakage was observed on any of the follow-up postoperative CT scans.

Clinical Course

The mean JOA score for lower-limb motor function was 1.8 ± 0.6 before surgery, 1.7 ± 0.6 at discharge, and 1.4 ± 0.7 at the most recent follow-up visit (Table 3). No patients exhibited neurological deterioration due to OPLL progression. One patient developed a severe gait disturbance due to an unrelated cause (worsening of lumbar canal stenosis), but the other 8 experienced gait disturbance improvements.

Illustrative Case

A 55-year-old woman presented with a walking disturbance and lower-extremity muscle weakness. She had mixed-type OPLL, extending from T-4 to T-10. The level of the most obvious protrusion was T5–6, with an OPLL area of 97.3 mm². We performed T2–10 laminectomy and posterior fixation from T-2 to T-12. Three years after surgery, the area of OPLL at T5–6 had increased to 113.9 mm² (Fig. 3).

TABLE 2: Area of thoracic OPLL at the level of the most obvious protrusion

Patient No.	Area of the OPLL (mm²)		Progression Rate (%)*
	Preop	At Last Follow-Up	
1	65.77	141.80	216
2	101.00	114.20	113
3	54.00	77.75	144
4	97.30	113.90	117
5	66.54	105.30	158
6	134.70	173.30	129
7	83.14	133.70	161
8	98.17	132.50	135
9	52.47	62.76	120

* The OPLL progression rate was determined by dividing the last follow-up area by the preoperative area.

Discussion

This is the first study to investigate the progression of thoracic OPLL after spinal stabilization. The use of thin-slice CT scans allowed us to conduct a detailed analysis of thoracic OPLL, which is difficult to do with plain radiographs. We found that the postoperative area of ossification increased both axially and longitudinally.

It is well recognized that cervical OPLL is progressive during the natural course of the disease and after decompressive surgery.[4–6,10,15] Several investigators have reported that ossification progression aggravates myelopathy, whereas others have found no relationship between neurological function deterioration and ossification progression.[2,5,7] This study is the first to show that ossification also progresses in the thoracic spine; however, this progression did not aggravate patients' myelopathy in the present series.

The pathomechanisms underlying the progression of OPLL remain unclear, but mechanical stress has been implicated as an exacerbating factor.[19] Our initial hypothesis was that spinal stabilization suppresses OPLL progression by eliminating local motion of the spine. Contrary to our hypothesis, we found that OPLL continued to progress after spinal stabilization. A study with a longer follow-up period may provide additional information regarding the time course of OPLL progression.

There are several limitations associated with this study that deserve mention. First, the number of patients examined in this study was small. However, our findings were consistent among the cohort. Similarly, the length of follow-up was relatively short. Although OPLL progression did not result in functional deterioration in the present study, such progression could manifest in neurological dysfunction over a longer time span. Finally, we did not measure local spinal motion. A previous study showed that dynamic factors, such as the segmental range of mo-

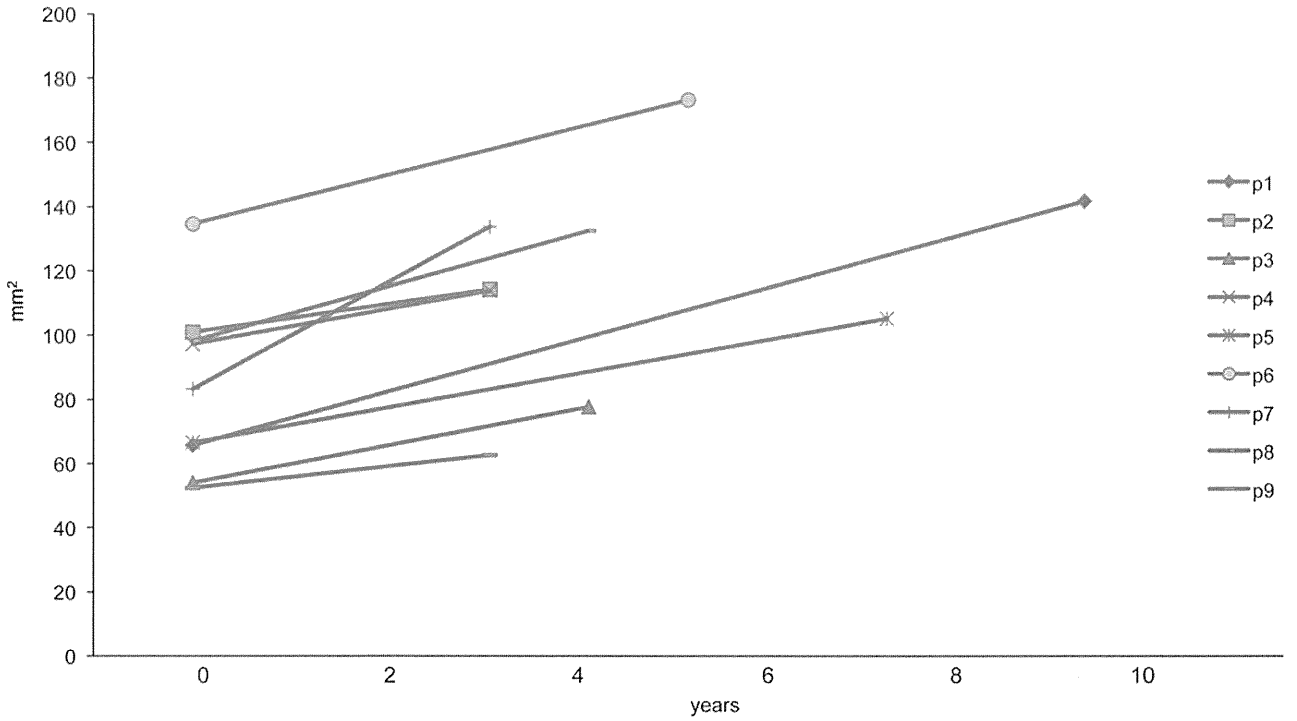

FIG. 2. Progression of OPLL during the follow-up period. The area of ossification increased in all patients. p = patient.

tion, contribute to the development of myelopathy in the cervical spine among patients with OPLL.[3] However, it is difficult to precisely measure local thoracic spine motion with plain radiographs. Notably, we observed neither screw loosening nor rod breakage on any of the follow-up CT scans, indicating that we successfully stabilized the patients' spines. A detailed analysis of spinal motion is needed in future studies.

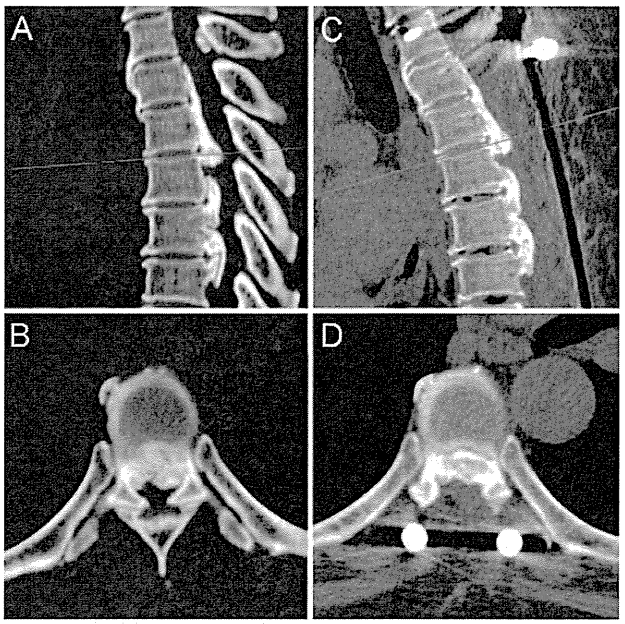

FIG. 3. **A:** The level of the most obvious protrusion of ossification was determined as previously described *(line)*. **B:** Preoperative axial view of ossification at the determined level. **C:** The same level was selected on postoperative CT scans. **D:** Axial postoperative CT scan showing enlargement of the area of ossification.

Conclusions

The present study demonstrated that thoracic OPLL does not decrease or stop and affects a larger area over time, even after spinal stabilization. Although OPLL progression did not result in functional deterioration in this study, physicians should pay attention to continued ossification in patients with thoracic OPLL.

Disclosure

The authors report no conflict of interest concerning the mate-

TABLE 3: JOA scores for lower-limb motor function in each patient

Patient No.	JOA Score		
	Preop	Postop	Last Follow-Up
1	3	3	2
2	2	2	1
3	2	2	2
4	2	2	2
5	1	1	1
6	2	2	2
7	1	1	0
8	1	1	1
9	2	2	2

rials or methods used in this study or the findings specified in this paper. This study was funded by a grant from the Ministry of Health, Labour, and Welfare of Japan (Research on Intractable Diseases grant no. H23-Nanchi-032). The funders played no role in the design of the study, data collection and analysis, decision to publish, or preparation of the manuscript.

Author contributions to the study and manuscript preparation include the following. Conception and design: Sugita, Chikuda. Acquisition of data: Sugita. Analysis and interpretation of data: Sugita. Drafting the article: Sugita. Critically revising the article: all authors. Reviewed submitted version of manuscript: all authors. Approved the final version of the manuscript on behalf of all authors: Sugita.

References

1. Fargen KM, Cox JB, Hoh DJ: Does ossification of the posterior longitudinal ligament progress after laminoplasty? Radiographic and clinical evidence of ossification of the posterior longitudinal ligament lesion growth and the risk factors for late neurologic deterioration. A review. **J Neurosurg Spine 17:**512–524, 2012
2. Fujimura Y, Nishi Y, Chiba K, Nakamura M, Hirabayashi K: Multiple regression analysis of the factors influencing the results of expansive open-door laminoplasty for cervical myelopathy due to ossification of the posterior longitudinal ligament. **Arch Orthop Trauma Surg 117:**471–474, 1998
3. Fujiyoshi T, Yamazaki M, Okawa A, Kawabe J, Hayashi K, Endo T, et al: Static versus dynamic factors for the development of myelopathy in patients with cervical ossification of the posterior longitudinal ligament. **J Clin Neurosci 17:**320–324, 2010
4. Inoue H, Ohmori K, Ishida Y, Suzuki K, Takatsu T: Long-term follow-up review of suspension laminotomy for cervical compression myelopathy. **J Neurosurg 85:**817–823, 1996
5. Iwasaki M, Kawaguchi Y, Kimura T, Yonenobu K: Long-term results of expansive laminoplasty for ossification of the posterior longitudinal ligament of the cervical spine: more than 10 years follow up. **J Neurosurg 96 (2 Suppl):**180–189, 2002
6. Kato Y, Iwasaki M, Fuji T, Yonenobu K, Ochi T: Long-term follow-up results of laminectomy for cervical myelopathy caused by ossification of the posterior longitudinal ligament. **J Neurosurg 89:**217–223, 1998
7. Kawaguchi Y, Kanamori M, Ishihara H, Nakamura H, Sugimori K, Tsuji H, et al: Progression of ossification of the posterior longitudinal ligament following en bloc cervical laminoplasty. **J Bone Joint Surg Am 83-A:**1798–1802, 2001
8. Kawahara N, Tomita K, Murakami H, Hato T, Demura S, Sekino Y, et al: Circumspinal decompression with dekyphosis stabilization for thoracic myelopathy due to ossification of the posterior longitudinal ligament. **Spine (Phila Pa 1976) 33:** 39–46, 2008
9. Matsumoto M, Toyama Y, Chikuda H, Takeshita K, Kato T, Shindo S, et al: Outcomes of fusion surgery for ossification of the posterior longitudinal ligament of the thoracic spine: a multicenter retrospective survey. Clinical article. **J Neurosurg Spine 15:**380–385, 2011
10. Matsunaga S, Kukita M, Hayashi K, Shinkura R, Koriyama C, Sakou T, et al: Pathogenesis of myelopathy in patients with ossification of the posterior longitudinal ligament. **J Neurosurg 96 (2 Suppl):**168–172, 2002
11. Matsunaga S, Sakou T: Ossification of the posterior longitudinal ligament of the cervical spine: etiology and natural history. **Spine (Phila Pa 1976) 37:**E309–E314, 2012
12. Matsuyama Y, Sakai Y, Katayama Y, Imagama S, Ito Z, Wakao N, et al: Indirect posterior decompression with corrective fusion for ossification of the posterior longitudinal ligament of the thoracic spine: is it possible to predict the surgical results? **Eur Spine J 18:**943–948, 2009
13. Min JH, Jang JS, Lee SH: Clinical results of ossification of the posterior longitudinal ligament (OPLL) of the thoracic spine treated by anterior decompression. **J Spinal Disord Tech 21:** 116–119, 2008
14. Murakami M, Seichi A, Chikuda H, Takeshita K, Nakamura K, Kimura A: Long-term follow-up of the progression of ossification of the posterior longitudinal ligament. Case report. **J Neurosurg Spine 12:**577–579, 2010
15. Ogawa Y, Toyama Y, Chiba K, Matsumoto M, Nakamura M, Takaishi H, et al: Long-term results of expansive open-door laminoplasty for ossification of the posterior longitudinal ligament of the cervical spine. **J Neurosurg Spine 1:**168–174, 2004
16. Ohtsuka K, Terayama K, Tsuchiya T, Wada K, Furukawa K, Ohkubu M: [A surgical procedure of the anterior decompression of the thoracic spinal cord through the posterior approach.] **Orthop Surg Traumatol 26:**1083–1090, 1983 (Jpn)
17. Seichi A, Hoshino Y, Ohnishi I, Kurokawa T: The role of calcium metabolism abnormalities in the development of ossification of the posterior longitudinal ligament of the cervical spine. **Spine (Phila Pa 1976) 17 (3 Suppl):**S30–S32, 1992
18. Suzuki K, Ishida Y, Ohmori K: Long term follow-up of diffuse idiopathic skeletal hyperostosis in the cervical spine. Analysis of progression of ossification. **Neuroradiology 33:**427–431, 1991
19. Tsukamoto N, Maeda T, Miura H, Jingushi S, Hosokawa A, Harimaya K, et al: Repetitive tensile stress to rat caudal vertebrae inducing cartilage formation in the spinal ligaments: a possible role of mechanical stress in the development of ossification of the spinal ligaments. **J Neurosurg Spine 5:**234–242, 2006
20. Yamazaki M, Mochizuki M, Ikeda Y, Sodeyama T, Okawa A, Koda M, et al: Clinical results of surgery for thoracic myelopathy caused by ossification of the posterior longitudinal ligament: operative indication of posterior decompression with instrumented fusion. **Spine (Phila Pa 1976) 31:**1452–1460, 2006

Manuscript submitted December 26, 2013.
Accepted July 7, 2014.
Please include this information when citing this paper: published online August 15, 2014; DOI: 10.3171/2014.7.SPINE131191.

Address correspondence to: Shurei Sugita, M.D., 7-3-1, Hongo, Bunkyo-ku, Tokyo 113-8655, Japan. email: ssugita-tky@umin.ac.jp.

Biomedical Research (Tokyo) **35** (4) 243-250, 2014

S100A1 and S100B are dispensable for endochondral ossification during skeletal development

Yoshifumi MORI[1], Daisuke MORI[2], Ung-il CHUNG[3], Sakae TANAKA[1], Jörg HEIERHORST[4], Thierry BUCHOU[5], Jacques BAUDIER[5], Hiroshi KAWAGUCHI[1, 6], and Taku SAITO[1, 2]

[1] Sensory & Motor System Medicine, [2] Bone and Cartilage Regenerative Medicine, [3] Center for Disease Biology and Integrative Medicine, Faculty of Medicine, University of Tokyo, 7-3-1 Hongo, Bunkyo-ku, Tokyo 113-8655, Japan; [4] St. Vincent's Institute of Medical Research, and Department of Medicine, St. Vincent's Hospital, The University of Melbourne, 9 Princes Street, Fitzroy, Victoria 3065, Australia; [5] Inserm, U823, Université Joseph Fourier-Grenoble 1, Institut Albert Bonniot, faculté de Médecine, La tronche, France; and [6] Spine Center, Tokyo Shinjuku Medical Center, Japan Community Health care Organization, 5-1 Tsukudotyo, Shinjuku-ku, Tokyo 162-8543, Japan

(Received 8 May 2014; and accepted 14 May 2014)

ABSTRACT

S100A1 and S100B are induced by the SOX trio transcription factors (SOX9, SOX5, and SOX6) in chondrocytes, and inhibit their hypertrophic differentiation in culture. However, functional roles of S100A1 and S100B during *in vivo* skeletal development are yet to be determined. Here we show that mice deficient of both the *S100a1* and *S100b* genes displayed normal skeletal growth from embryonic stage to adulthood. Although no compensatory upregulation of other S100 family members was observed in *S100a1/S100b* double mutants, the related *S100a2*, *S100a4*, *S100a10*, and *S100a11* were expressed at similarly high levels to *S100a1* and *S100b* in mouse primary chondrocytes. Furthermore, overexpression of these other S100 members suppressed the hypertrophic differentiation of chondrocytes *in vitro* as efficiently as S100A1 and S100B. Taken together, the present study demonstrates that S100A1 and S100B are dispensable for endochondral ossification during skeletal development, most likely because their deficiency may be masked by other S100 proteins which have similar functions to those of S100A1 and S100B.

Endochondral ossification is fundamental process for skeletal development. In this process, chondrocytes derived from condensed mesenchymal cells undergo proliferation and differentiation into hypertrophic cells. In the terminal stage, the hypertrophic chondrocytes mineralize a surrounding matrix to provide a scaffold for osteoblasts. The sex determining region Y-type high mobility group box (SOX) family transcription factors play essential roles for these differentiation steps of chondrocytes (1, 2). SOX9 is indispensable for mesenchymal condensation and the subsequent early stage of chondrocyte differentiation (9, 15, 21). SOX5 and SOX6 function as co-activators of SOX9 in chondrocyte differentiation (13, 19). In addition to their stimulatory effect for early stage of chondrocyte differentiation, the SOX trio (SOX9, SOX5, and SOX6) exert inhibitory effects on chondrocyte hypertrophy (1).

S100 proteins form a subgroup of the superfamily of Ca^{2+}-binding protein with EF-hand motif (3). This subgroup consists of over 20 family members (3). S100 family members are low molecular weight proteins, and differentially expressed in normal and transformed cells (6). Intracellular S100 proteins usually function as modulators of their target proteins, and exert various roles such as regulation of

Address correspondence to: Taku Saito, M.D., Ph.D., Associate Professor
Bone and Cartilage Regenerative Medicine, Faculty of Medicine, University of Tokyo, Hongo 7-3-1, Bunkyo-ku, Tokyo 113-8655, Japan
Tel: +81-3-3815-5411 (ext. 37369), Fax: +81-3-3818-4082
E-mail: tasaitou-tky@umin.ac.jp

protein phosphorylation, enzyme activity, Ca^{2+} homeostasis, cytoskeleton components, and transcription factors (6). Some S100 proteins can be secreted and involved with extracellular activities such as regulation of the nervous system and inflammation (6).

Previously, we have identified S100A1 and S100B as direct transcriptional targets of the SOX trio (17). S100A1 and S100B are abundantly expressed in the prehypertrophic and hypertrophic chondrocyte zones of mouse embryonic limb cartilage (17). During differentiation of the mouse chondrocytic cell line ATDC5, S100A1 and S100B exhibit a similar inhibitory effect on hypertrophic differentiation, meanwhile they have no obvious effect on chondrogenic differentiation and cartilage matrix production (17). However, functions of S100A1 and S100B *in vivo* still remain unknown. Furthermore, expression of whole S100 family members in chondrocytes during endochondral ossification has not been revealed. In the present study, we sought to examine the role of S100A1 and S100B in the regulation of normal skeletal development using mice in which both genes had been deleted, and further examined compensatory effects by other S100 family members.

MATERIALS AND METHODS

Mice. *S100a1* and *S100b* knockout (KO) mice were previously generated as described (7, 22). We intercrossed mice heterozygous for *S100a1* (*S100a1+/−*) and mice heterozygous for *S100b* (*S100b+/−*) to obtain compound *S100a1+/−; S100b+/−* heterozygotes, which were then mated with each other and their offspring was used for analyses. Genomic DNA obtained from embryonic membrane (E12.5), unilateral upper and lower extremity (E16.5), or tail (postnatal) was used for genotyping PCR using KOD-FX (TOYOBO) with primers, annealing temperature, and cycle numbers listed in Table 1.

Histological and radiological analyses. We stained whole skeletons of E12.5 embryos with Alcian blue (12). We analyzed skeletons of E16.5 embryos by staining with Alizarin red and Alcian blue as described previously (11). Photographs of unstained whole bodies (E16.5) and stained skeletons (E12.5 and E16.5) were taken using digital microscopy (VH-5500, KEYENCE). We took plain whole body radiographs of 8-week-old mice using a soft x-ray apparatus (Softex CMB-2, SOFTEX). We measured lengths of humerus, ulna, femur, tibia, and lumbar spine (L1 to L6) on photographs of doube-stained skeletons (E16.5) or radiographs (8-week-old). Bone length of 8-week-old mice was then normalized to sex-matched *S100a1+/−; S100b+/−* littermates to correct for sex-related difference. Under deep anesthesia, 1-day-old and 8-week-old mice were transcardially perfused with PBS followed by 4% paraformaldehyde phosphate buffer solution (PFA/PBS). Then, we harvested lower extremities of 1-day-old mice and humerus of 8-week-old mice, and fixed them further in 4% PFA/PBS for 2 days. We decalcified the latter in 10% EDTA at 20°C for one week. They were then embedded in paraffin, and cut into 10 μm sections. H&E, Toluidine blue, and von Kossa staining were performed according to standard protocols.

Construction of expression vectors. We prepared expression vectors in pShuttle (Clontech) and pcDNA3.1(+) (Invitrogen). We verified all cDNA inserts by DNA sequencing.

Cell cultures. ATDC5 cells (Riken BRC) were maintained in DMEM/Ham's F-12 (1 : 1) (Wako) containing 5% FBS, penicillin (100 U/mL), and streptomycin (100 μg/mL). ATDC5 cells were plated at 1×10^5 cells/well on 6-well plates 1 day before transfection. In each well, 2 μg of each expression vector was transfected using 3.5 μL Lipofectamine 2000 (Life technologies). One day after the transfection, cells were detached and cultured in pellet for an additional 5-day period.

Real-time RT-PCR. We harvested rib cartilage from 8-week-old mice. To remove attached soft tissue, we digested the harvested cartilage tissues with 0.3%

Table 1 *List of primers used for genotyping*

Gene	Genotype	Forward primer	Reverse primer	Product size (bp)	Annealing Temperature (°C)	Cycle
S100a1	WT	TCTCCATTCTCCCACTCTCG	CTTAGCTTCTGGGCAGTCGT	394	62	35
	null	GAGAATGGTAACCGAGCCGCCC	AGGTGTTGGGAGTGAGCACCC	300	62	33
S100b	WT	GGGATGGCACCACCCACAATGG	TCTGGTGGCTATTCCCAATCCC	400	60	35
	null	GATCGGCCATTGAACAAGAT	CTCGTCCTGCAGTTCATTCA	194	64	33

collagenase (WAKO) for 2 h at 37°C, and washed twice with PBS. The cartilage tissues were homogenized using Precellys24 tissue homogenizer (Bertin laboratories), and total RNA was purified from the lysates using RNeasy mini kits (Qiagen) according to the manufacturer's protocol. From pellet-cultured ATDC5 cells, we extracted total RNA by RNeasy mini kit as well. We reverse-transcribed 1 μg of total RNA with QuantiTect RT kit (Qiagen) according to the manufacturer's protocol. Real-time RT-PCR was performed on a Thermal Cycler Dice (Takara) using FastStart Universal SYBR Green Master (Roche). The full-length or partial-length cDNAs of target genes, including PCR amplicon sequences, were amplified by PCR, cloned into pCR-TOPO Zero II or pCR-TOPO II vectors (Invitrogen), and used as standard templates after linearization. Copy numbers of target mRNA in each total RNA were calculated by reference to standard curves and were adjusted to the mouse standard total RNA (ABI) with the rodent *Gapdh* as an internal control. Primer information is listed in Table 2.

Statistical analysis. Differences between two groups were analyzed by student's *t*-test. Differences among multiple groups were analyzed by one-way ANOVA followed by Holm's *t*-test. $P < 0.05$ was considered significant.

RESULTS

Skeletal development of S100A1 and S100B null mice Since S100A1 and S100B have similar functions in chondrocyte differentiation *in vitro* (17) and homozygous *S100a1* or *S100b* KO mutants showed no obvious abnormality during skeletal development (7, 22), we generated double KO (DKO) mutants for both *S100a1* and *S100b* by intercrossing the two mouse lines. Compound heterozygous *S100a1+/−; S100b+/−* founders showed normal skeletal growth compared to wild-type mice (*S100a1+/+; S100b+/+*, WT) at birth (data not shown). Further mating revealed that all homozygous double mutants lacking both S100A1 and S100B proteins (*S100a1−/−; S100b−/−*, DKO) grew normally without obvious abnormality in embryonic stages (Fig. 1A, B). Double staining of skeletons of WT and DKO neonates with Alizarin red and Alcian blue confirmed the similar development of limbs and vertebrae (Fig. 1C, D). Histological analyses including H&E and von Kossa staining failed to detect obvious differences in the architecture of chondrocyte differentiation zones and mineralization between the different genotypes (Fig. 1E, F).

Table 2 *List of primers used for real-time RT-PCR*

Gene	Species	Forward primer	Reverse primer	Product size (bp)
Gapdh	Mouse	TGCACCACCAACTGCTTAGC	GGATGCAGGGATGATGTTCT	177
S100a1	Mouse	GACAAGGTAATGAAGGAACTGGATG	TGAGGAGCAAGCACGCTAAA	190
S100a2	Mouse	CGTAGATGATGAGAAGGTGA	CAGAACCAGGGCATACATC	91
S100a3	Mouse	TGAGTGTTCTGGATACCAACAAAGA	GGACAAAGATGGAGGACTGGA	197
S100a4	Mouse	CTTCCTCTCTCTTGGTCTGGTCTC	AACTTCATTGTCCCTGTTGCTGT	244
S100a5	Mouse	GCAGAGAAGATGAAGGAGAGCA	CCATAGGAGGGGCAGTTAAAGA	211
S100a6	Mouse	GTGCCAGAAGGGAAAACTAAACAC	GAGGCAAGGCAAACGAACA	180
S100a8	Mouse	AGGAAATCACCATGCCCTCTAC	GCCACACCCACTTTTATCACC	174
S100a9	Mouse	AGCGCAGCATAACCACCA	CATCAGCATCATACACTCCTCAAA	224
S100a10	Mouse	GAAGCAGAAGGGGAAGAAGTAGG	TTTATTGAGGGCAATGGGATG	238
S100a11	Mouse	CGCATGATGAAGAAGCTGGA	GATGACTTGGTGGTTGGATGG	162
S100a13	Mouse	GCTGTGTTGGGATGGCTAGTG	CGGGAAAGAAGGTGGGATG	157
S100a14	Mouse	GTAGGGGAAGGGCAGAAAGG	AGGATAGCACAGGGCAGACAA	157
S100a16	Mouse	CAACCTCATCCGCCAACA	GGGAGAAGGGAGGAAGAAAGAG	196
S100a17	Mouse	AATGAAGAAGGTGAGGTAGGTGATG	TGTGTTGGACTGGTGCTCTGT	227
S100a18	Mouse	AACTAAGAAAAGGGAAGGAGCAAAG	CAGGTTGAGGGAAGCCAGA	168
S100b	Mouse	GCCCACACCCAGTTCTCTCT	CTGACTTCTTCAGCTTGTGCTTG	211
S100g	Mouse	CTGGATAAGAATGGCGATGGA	GACGTGTCTCCGAACTTGCTT	193
S100z	Mouse	ACCATGATTCGCATCTTCCAC	GTCCTGCATTATCTTATCCACCAAC	153
Col10a1	Mouse	CATAAAGGGCCCACTTGCTA	TGGCTGATATTCCTGGTGGT	224
Runx2	Mouse	CCCAGCCACCTTTACCTACA	TATGGAGTGCTGCTGGTCTG	150
Pth1r	Mouse	GGGCACAAGAAGTGGATCAT	GGCCATGAAGACGGTGTAGT	210

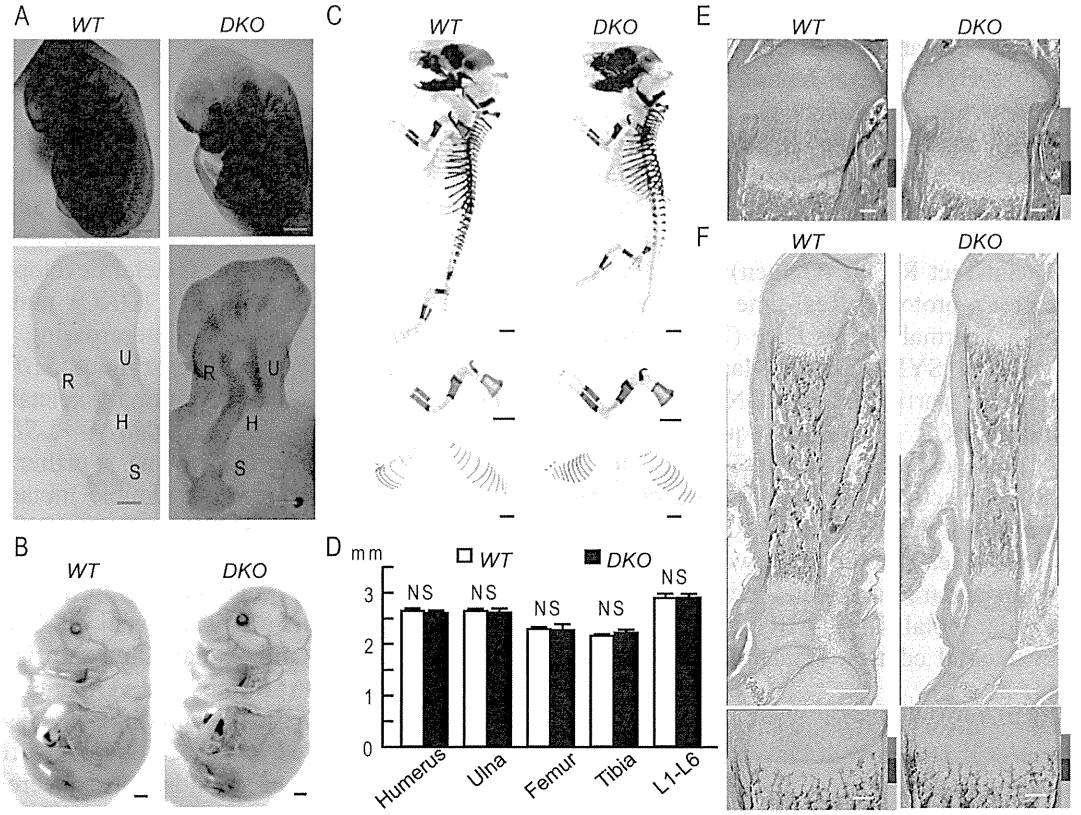

Fig. 1 Skeletal development of *S100a1–/–; S100b–/–* (DKO) mice from embryonic stage to the perinatal period. (**A**) Alcian blue staining of *S100a1+/+; S100b+/+* (WT) and DKO embryos (E12.5). R, radius; U, ulnar; H, humerus; S, scapula. Scale bars, 1 mm (top), 200 μm (bottom). (**B**) Gross appearance of WT and DKO littermate embryos (E16.5). Scale bars, 1 mm. (**C**) Double staining with Alizarin red and Alcian blue of the whole skeleton (top), upper extremities (middle), and ribs (bottom) of WT and DKO littermate embyos (E16.5). Scale bars, 1 mm. (**D**) Length of long bones and vertebra (first to sixth lumbar spines) of WT and DKO mice (E16.5). All data are means ± SD of three mice per group. NS, no significant difference. (**E**) H&E staining of proximal tibias of WT and DKO neonates. Scale bars, 100 μm. Right bars indicate length of proliferative zone (red), hypertrophic zone (blue), and bone area (green). (**F**) von Kossa staining of whole tibias (top) and distal femurs (bottom) of WT and DKO neonates. Scale bars, 500 μm (top), 100 μm (bottom). Right bars indicate length of proliferative zone (red), hypertrophic zone (blue), and bone area (green).

Up to adulthood, DKO mice showed normal skeletal growth, compared to WT mice (Fig. 2A, B). H&E and Toluidine blue stainging confirmed the similar architecture of articular cartilage in WT and DKO knee joints (Fig. 2C). Besides the skeletal development, DKO mice did not show obvious abnormality in appearance and behavior up to 24 months old.

Expressions of S100 protein family members in chondrocytes

To assess whether other S100 proteins may compensate for the deficiency of S100a1 and S100b in skeletal development, we next examined expression levels of other family members in chondrocytes obtained from WT, S100a1 null mice (*S100a1−/−; S100b+/+*, a1KO), S100b null mice (*S100a1+/+; S100b−/−*, bKO), and DKO mice. Although loss of *S100a1* and/or *S100b* mRNAs was confirmed in the respective mutants, compensatory upregulation of other S100 family members was not observed (Fig. 3). When we compared mRNA expression levels of the S100 family members, several members including *S100a2, S100a4, S100a10, S100a11* showed high expression levels that were in a comparable range to those of *S100a1* and *S100b* in WT tissues (Fig. 3).

Suppression of the hypertrophic differentiation of chondrocytes by S100 family members

We next examined whether the other S100 family members which are physiologically abundantly expressed in chondrocytes may suppress the hypertrophic differentiation of chondrocytes similarly to S100A1 and S100B. When we overexpressed S100A1, S100B, S100A2, S100A4, S100A10, S100A11, or

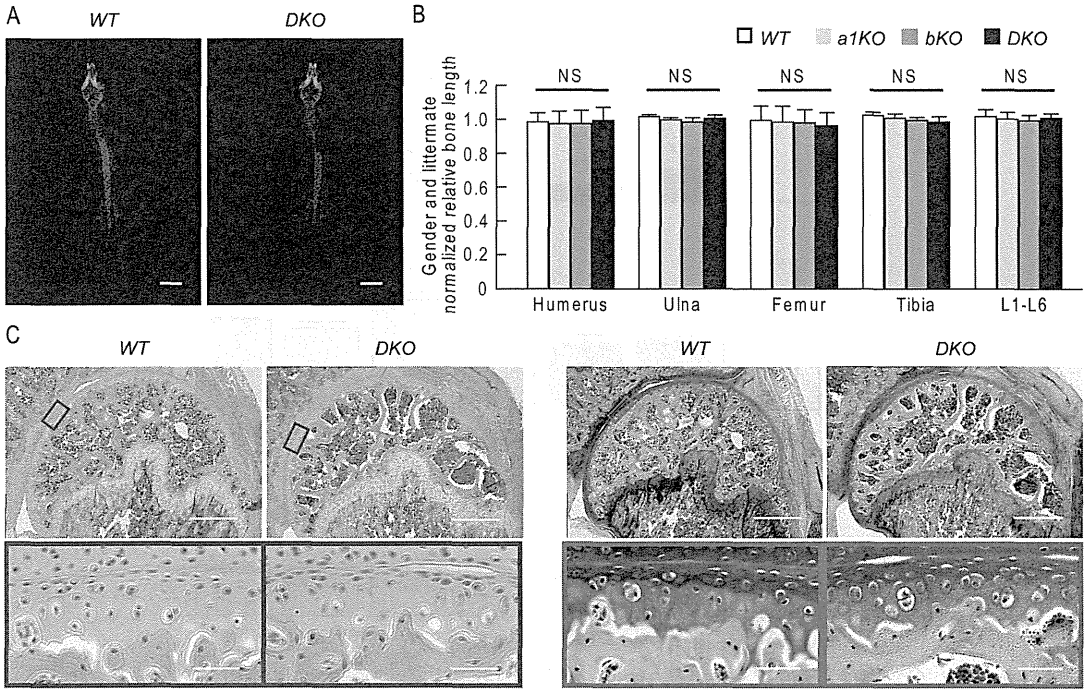

Fig. 2 Skeletal development of DKO mice in the postnatal period. (**A**) Plain radiographs of the entire bodies of WT and DKO littermates (8-week-old). Scale bars, 1 cm. (**B**) Length of long bones and vertebra (first to sixth lumbar spines) of WT (n = 4), *S100a1−/−; S100b+/+* (a1KO, n = 7), *S100a1+/+; S100b−/−* (bKO, n = 3), and DKO (n = 7) mice (8-week-old). All Data are shown as means ± SD. NS, no significance. (**C**) H&E staining (left) and Toluidine blue staining (right) of glenohumeral joints of WT and DKO mice (8-week-old). Scale bars, 500 μm (top), 50 μm (bottom).

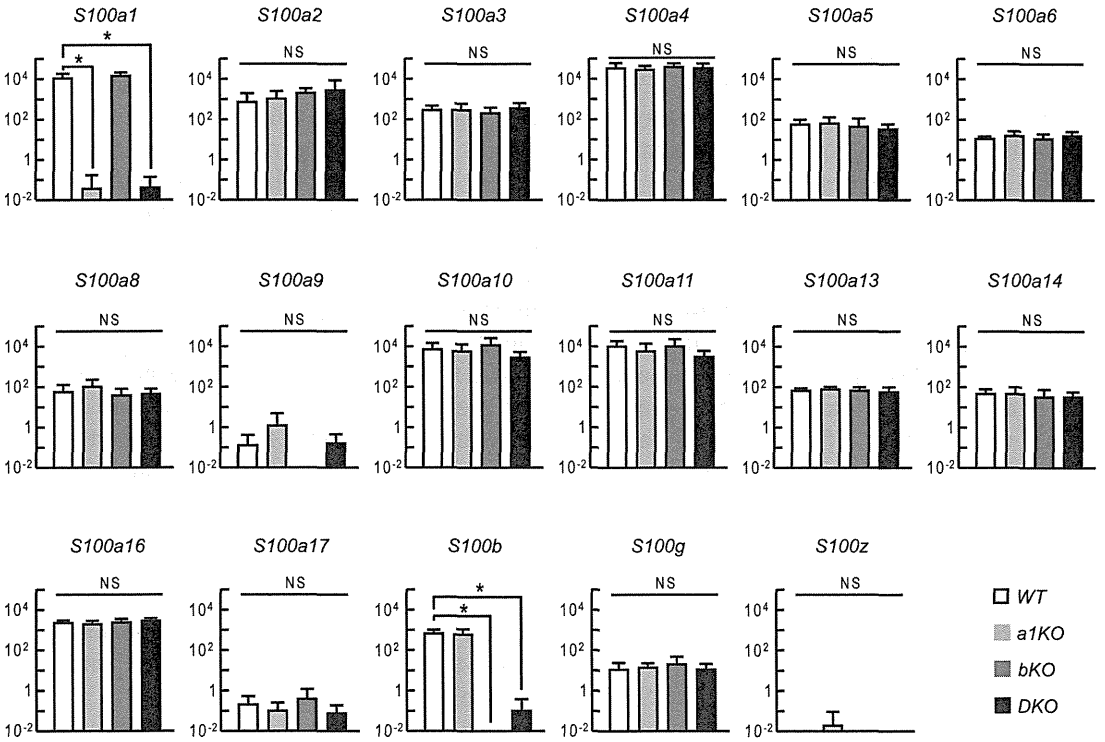

Fig. 3 mRNA levels of S100 family members in rib cartilage obtained from WT (n = 8), a1KO (n = 10), bKO (n = 5), and DKO (n = 6) mice. All Data are shown as means ± SD. *$P < 0.05$. NS, no significant difference.

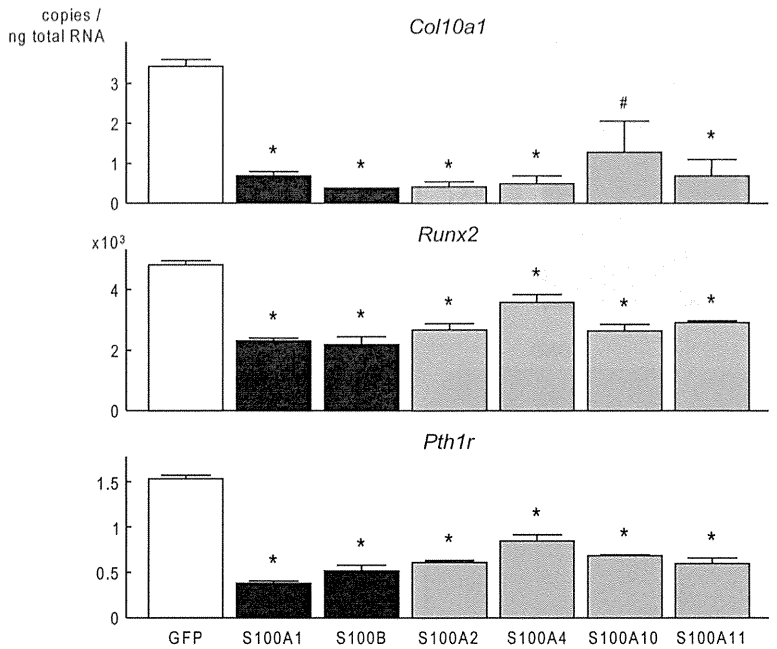

Fig. 4 mRNA levels of *Col10a1, Runx2, and Pth1r* in ATDC5 cells transduced with GFP, S100A1, S100B, S100A2, S100A4, S100A10 and S100A11 expressing vectors after 5-day-pellet culture. All data are shown as means ± SD of three samples per group. $^{\#}P < 0.05$, $^{*}P < 0.01$, versus GFP.

GFP in a mouse chondrogenic cell line ATDC5 by lipofection and cultured them in pellet for 5 days, representative marker genes for hypertrophic differentiation of chondrocytes, including type 10 collagen (*Col10a1*), runt related transcription factor 2 (*Runx2*), and parathyroid hormone 1 receptor (*Pth1r*) were significantly decreased by overexpression of other S100 family members, to a level comparable to S100A1 or S100B overexpression (Fig. 4).

DISCUSSION

The present study using double mutant mice deficient of both *S100a1* and *S100b* shows that these two S100 proteins are dispensable for normal endochodral ossification during skeletal development. Compensatory upregulation of other S100 family members was not observed in *S100a1/b* double mutants; however, *S100a2*, *S100a4*, *S100a10*, and *S100a11* are abundantly expressed in cartilage tissue, at levels similar to *S100a1* and *S100b*. These S100 proteins suppressed the hypertrophic differentiation as efficiently as S100A1 and S100B in gain-of-function analysis using ATDC5 cells. Collectively, these data indicate that deficiency of *S100a1* and *S100b* may be masked by these other four S100 proteins. Consistent with our results, stress situations were necessary to reveal phenotypes of S100 KO mice, since S100 proteins are often upregulated in pathogenic situation including cancers, inflammation, and other cellular stress (4, 7, 8, 10, 14, 22).

Despite the data presented here for skeletal development, there is increasing evidence for the expression and function of S100 family members in articular cartilage. A recent study reports that S100A1 and S100B are useful as markers to evaluate human articular chondrocyte (HAC) differentiation status (5). In that report, *S100A1* and *S100B*, as well as cartilage matrix genes including *COL2A1* and *ACAN*, were downregulated during dedifferentiation of HAC. In contrast, *S100A1* and *S100B* were upregulated during redifferentiation of HAC, simultaneously with *COL2A1* and *ACAN*. These data are compatible with our previous findings that *S100A1* and *S100B* together with *COL2A1* and *ACAN* are direct transcriptional target genes of the key chondrogenic regulators SOX9, SOX5, and SOX6. Notably, *S100A10* was expressed in HACs regardless of their dedifferentiation status (5). Although expression of other S100 family members besides *S100A1* and *S100B* may not be regulated in the same manner in chondrocytes, they could still partially compensate for functions of S100A1 and S100B.

Two other S100 family members, S100A8 and S100A9, are known as catabolic factors for articular cartilage. Although expression levels of *S100a8* and

S100a9 were lower than those of *S100a1* and *S100b* in rib cartilage, *S100a8* and *S100a9* are expressed in inflamed synovia, and *S100a9* null mice showed resistance to joint inflammation and articular cartilage destruction during antigen-induced inflammatory arthritis (20). Intra-articular injection of S100a8 caused prominent joint inflammation with upregulation of matrix metallopeptidases (20). In a surgically-induced osteoarthritis model, *S100a8* and *S100a9* were upregulated in early stage of osteoarthritis development (23). In human articular chondrocytes, *S100A8* and *S100A9* were associated with expression of cartilage degradation markers and induction of catabolic factors and suppression of anabolic factors (18). Meanwhile, S100A1 and S100B suppress the hypertrophic differentiation of chondrocytes, which is essential in osteoarthritis development as well as in skeletal development (16, 17). Considering that S100A8 and S100A9 exert their catabolic effect as secreted proteins, intracellular and extracellular functions of S100 family members may not be same.

In conclusion, DKO mice displayed normal skeletal growth, which may be due to functions of other S100 family members similar to those of S100A1 and S100B. Elucidation of overlapped functions and expressions of S100 family members may be essential to understand their complicated roles *in vivo*.

Acknowledgments

We thank J Sugita, R. Yamaguchi and H. Kawahara for technical assistance. This study was supported by a Grant-in-aid for Scientific Research from the Japanese Ministry of Education, Culture, Sports, Science and Technology (#23390358, 25462359). JH is supported by grants and a Senior Research Fellowship from the National Health and Medical Research Council of Australia, and in part by the Victorian State Government's Operational Infrastructure Support Porgram.

REFERENCES

1. Akiyama H, Chaboissier MC, Martin JF, Schedl A and de Crombrugghe B (2002) The transcription factor Sox9 has essential roles in successive steps of the chondrocyte differentiation pathway and is required for expression of Sox5 and Sox6. *Genes Dev* **16**, 2813–2828.
2. Bi W, Huang W, Whitworth DJ, Deng JM, Zhang Z, Behringer RR and de Crombrugghe B (2001) Haploinsufficiency of Sox9 results in defective cartilage primordia and premature skeletal mineralization. *Proc Natl Acad Sci USA* **98**, 6698–6703.
3. Chen H, Xu C, Jin Q and Liu Z (2014) S100 protein family in human cancer. *Am J Cancer Res* **4**, 89–115.
4. Deloulme JC, Raponi E, Gentil BJ, Bertacchi N, Marks A, Labourdette G and Baudier J (2004) Nuclear expression of S100B in oligodendrocyte progenitor cells correlates with differentiation toward the oligodendroglial lineage and modulates oligodendrocytes maturation. *Mol Cell Neurosci* **27**, 453–465.
5. Diaz-Romero J, Quintin A, Schoenholzer E, Pauli C, Despont A, Zumstein MA, Kohl S and Nesic D (2014) S100A1 and S100B expression patterns identify differentiation status of human articular chondrocytes. *J Cell Physiol* **229**, 1106–1117.
6. Donato R (2001) S100: a multigenic family of calcium-modulated proteins of the EF-hand type with intracellular and extracellular functional roles. *Int J Biochem Cell Biol* **33**, 637–668.
7. Du XJ, Cole TJ, Tenis N, Gao XM, Kontgen F, Kemp BE and Heierhorst J (2002) Impaired cardiac contractility response to hemodynamic stress in S100A1-deficient mice. *Mol Cell Biol* **22**, 2821–2829.
8. Eckert RL, Broome AM, Ruse M, Robinson N, Ryan D and Lee K (2004) S100 proteins in the epidermis. *J Invest Dermatol* **123**, 23–33.
9. Foster JW, Dominguez-Steglich MA, Guioli S, Kwok C, Weller PA, Goodfellow PN and Brook JD (1994) Campomelic dysplasia and autosomal sex reversal caused by mutations in an SRY-related gene. *Nature* **372**, 525–530.
10. Gilquin B, Cannon BR, Hubstenberger A, Moulouel B, Falk E, Merle N, Assard N, Kieffer S, Rousseau D, Wilder PT, Weber DJ and Baudier J (2010) The calcium-dependent interaction between S100B and the mitochondrial AAA ATPase ATAD3A and the role of this complex in the cytoplasmic processing of ATAD3A. *Mol Cell Biol* **30**, 2724–2736.
11. Itoh S, Saito T, Hirata M, Ushita M, Ikeda T, Woodgett JR, Algul H, Schmid RM, Chung UI and Kawaguchi H (2012) GSK-3alpha and GSK-3beta proteins are involved in early stages of chondrocyte differentiation with functional redundancy through RelA protein phosphorylation. *J Biol Chem* **287**, 29227–29236.
12. Jegalian BG and De Robertis EM (1992) Homeotic transformations in the mouse induced by overexpression of a human Hox3.3 transgene. *Cell* **71**, 901–910.
13. Lefebvre V, Li P and de Crombrugghe B (1998) A new long form of Sox5 (L-Sox5), Sox6 and Sox9 are coexpressed in chondrogenesis and cooperatively activate the type II collagen gene. *EMBO J* **17**, 5718–5733.
14. Marenholz I, Heizmann CW and Fritz G (2004) S100 proteins in mouse and man: from evolution to function and pathology (including an update of the nomenclature). *Biochem Biophys Res Commun* **322**, 1111–1122.
15. Ng LJ, Wheatley S, Muscat GE, Conway-Campbell J, Bowles J, Wright E, Bell DM, Tam PP, Cheah KS and Koopman P (1997) SOX9 binds DNA, activates transcription, and coexpresses with type II collagen during chondrogenesis in the mouse. *Dev Biol* **183**, 108–121.
16. Saito T, Fukai A, Mabuchi A, Ikeda T, Yano F, Ohba S, Nishida N, Akune T, Yoshimura N, Nakagawa T, Nakamura K, Tokunaga K, Chung UI and Kawaguchi H (2010) Transcriptional regulation of endochondral ossification by HIF-2alpha during skeletal growth and osteoarthritis development. *Nat Med* **16**, 678–686.
17. Saito T, Ikeda T, Nakamura K, Chung UI and Kawaguchi H (2007) S100A1 and S100B, transcriptional targets of SOX trio, inhibit terminal differentiation of chondrocytes. *EMBO*